NAVAL POSTGRADUATE SCHOOL
Monterey, California

AD-A232 248

DTIC
S ELECTE
MAR 0 5 1991
B D

THESIS

SEA ICE CLASSIFICATION
USING
SYNTHETIC APERTURE RADAR

by

Frank W. Garcia, Jr.

June, 1990

Thesis Advisors: J.A. Nystuen
                                                    R.H. Bourke

91 2 28 055

NAVAL POSTGRADUATE SCHOOL
Monterey, California

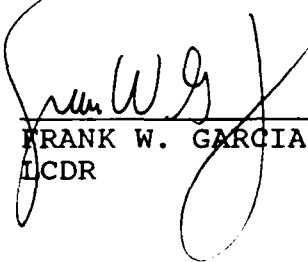Rear Admiral R. W. West, Jr.   Harrison Shull
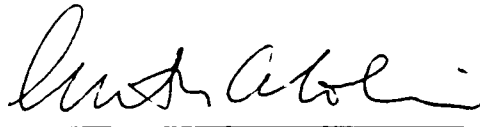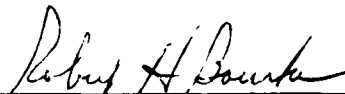Superintendent   Provost

This report was prepared in conjunction with research sponsored by the Naval Oceanographic and Atmospheric Research Laboratory, Ocean Sensing and Prediction Division, Remote Sensing Branch, Stennis Space Center, Mississippi and funded by the Naval Postgraduate School.

Reproduction of all or part of this report is authorized.

This report was prepared by:

_____
FRANK W. GARCIA Jr.
LCDR   USN

_____   _____
Reviewed by: Released by:

CURTIS A.COLLINS
Chairman
Department of Oceanography

REPORT DOCUMENTATION PAGE

1a REPORT SECURITY CLASSIFICATION UNCLASSIFIED	1b RESTRICTIVE MARKINGS

2a SECURITY CLASSIFICATION AUTHORITY	3 DISTRIBUTION/AVAILABILITY OF REPORT
2b DECLASSIFICATION/DOWNGRADING SCHEDULE	Approved for public release, distribution is unlimited.

4 PERFORMING ORGANIZATION REPORT NUMBER(S) NPS-68-90-004	5 MONITORING ORGANIZATION REPORT NUMBER(S)

6a NAME OF PERFORMING ORGANIZATION Naval Postgraduate School	6b OFFICE SYMBOL (If applicable) OC/Ny	7a NAME OF MONITORING ORGANIZATION Naval Postgraduate School

6c ADDRESS (City, State, and ZIP Code) Monterey, CA 93943-5000	7b ADDRESS (City, State, and ZIP Code) Monterey, CA 93943-5000

8a NAME OF FUNDING/SPONSORING ORGANIZATION; NAVAL OCEANOGRAPHIC AND ATMOSPHERIC RESEARCH LABORATORY	8b OFFICE SYMBOL CODE 321	9 PROCUREMENT INSTRUMENT IDENTIFICATION NUMBER O&MN, Direct Funding

8c ADDRESS (City, State, and ZIP Code),
OCEAN SENSING AND PREDICTION DIVISION,
REMOTE SENSING BRANCH,
STENNIS SPACE CENTER, MS 39529-5004

10 SOURCE OF FUNDING NUMBERS

Program Element No.	Project No.	Task No.	Work Unit Accession Number

11 TITLE (Include Security Classification)
SEA ICE CLASSIFICATION USING SYNTHETIC APERTURE RADAR

12 PERSONAL AUTHOR(S) Frank W. Garcia, Jr.

13a TYPE OF REPORT Master's Thesis	13b TIME COVERED From To	14 DATE OF REPORT (year, month, day) June 1990	15 PAGE COUNT 116

16 SUPPLEMENTARY NOTATION
The views expressed in this thesis are those of the author and do not reflect the official policy or position of the Department of Defense or the U.S. Government.

17 COSATI CODES			18 SUBJECT TERMS (continue on reverse if necessary and identify by block number)
FIELD	GROUP	SUBGROUP	Synthetic Aperture Radar Sea Ice Classification Marginal Ice Zone
			Gray Level Co-Occurrence Matrices Texture Statistics
			Univariate Statistics MIZEX '87 SAR Data

19 ABSTRACT (continue on reverse if necessary and identify by block number)

This study employs Synthetic Aperture Radar (SAR) imagery from the Marginal Ice Zone Experiment (MIZEX) 1987 to identify an optimal set of statistical descriptors that accurately classify three types of ice (first-year, multiyear, odden) and open water. Two groups of statistics, univariate and texture, are compared and contrasted with respect to their skill in classifying the ice types and open water. Individual statistical descriptors are subjected to principal component analysis and discriminant analysis. Principal component analysis was of little use in understanding features of each ice and open water group. Discriminant analysis was valuable in identifying which statistics held the most discriminating power. When combined, univariate and texture statistics classified the groups with 89.5% accuracy, univariate alone with 86.8% accuracy and texture alone with 75.4% accuracy. Range and inertia were the strongest univariate and texture discriminators with 74.6% and 50.8% accuracy, respectively. Despite the use of a non-calibrated SAR, univariate statistics were able to classify the images with greater accuracy than texture statistics.

20 DISTRIBUTION/AVAILABILITY OF ABSTRACT [X] UNCLASSIFIED/UNLIMITED [ ] SAME AS REPORT [ ] DTIC USERS	21 ABSTRACT SECURITY CLASSIFICATION UNCLASSIFIED
22a NAME OF RESPONSIBLE INDIVIDUAL J.A. Nystuen	22b TELEPHONE (Include Area code) (408) 646-2917 22c OFFICE SYMBOL OC/Ny

DD FORM 1473, 84 MAR   83 APR edition may be used until exhausted   SECURITY CLASSIFICATION OF THIS PAGE
All other editions are obsolete   UNCLASSIFIED

i

Sea Ice Classification
Using
Synthetic Aperture Radar

by

Frank W. Garcia, Jr.
Lieutenant Commander, United States Navy
B.S., University of South Carolina, 1979

Submitted in partial fulfillment
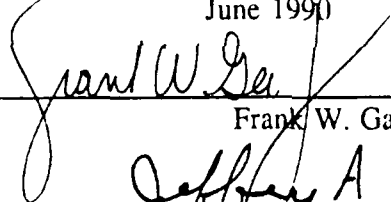of the requirements for the degree of

MASTER OF SCIENCE IN METEOROLOGY AND PHYSICAL OCEANOGRAPHY
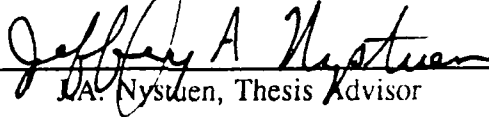
from the

NAVAL POSTGRADUATE SCHOOL
June 1990

Author: _____
Frank W. Garcia, Jr.

Approved by: _____
J.A. Nystuen, Thesis Advisor

_____
R.H. Bourke, Co-Advisor

_____
C.A. Collins, Chairman
Department of Oceanography

ABSTRACT

This study employs Synthetic Aperture Radar (SAR) imagery from the Marginal Ice Zone Experiment (MIZEX) 1987 to identify an optimal set of statistical descriptors that accurately classify three types of ice (first-year, multiyear, odden) and open water. Two groups of statistics, univariate and texture, are compared and contrasted with respect to their skill in classifying the ice types and open water. Individual statistical descriptors are subjected to principal component analysis and discriminant analysis. Principal component analysis was of little use in understanding features of each ice and open water group. Discriminant analysis was valuable in identifying which statistics held the most discriminating power. When combined, univariate and texture statistics classified the groups with 89.5% accuracy, univariate alone with 86.8% accuracy and texture alone with 75.4% accuracy. Range and inertia were the strongest univariate and texture discriminators with 74.6% and 50.8% accuracy, respectively. Despite the use of a non-calibrated SAR, univariate statistics were able to classify the images with greater accuracy than texture statistics.

iii

Accession For

NTIS GRA&I	☑
DTIC TAB	☐
Unannounced	☐
Justification	

By

Distribution/

Availability Codes

| Dist | Avail and/or Special |

TABLE OF CONTENTS

LIST OF TABLES

LIST OF FIGURES

ACKNOWLEDGEMENTS

I. INTRODUCTION

The polar regions remain one of the least explored areas on earth. The inhospitable environment of the polar region has severely hampered our ability to make prolonged observations and unravel it's many mysteries. A better understanding of the polar region is important because of this region's impact on global climate, sea level variation, ocean circulation and the great biological richness and commercial potential it holds. Recent technological advances, especially in remote sensing, have begun to allow some of the mysteries of the polar regions to be explained.

Remote sensing platforms have been in orbit providing limited coverage of the polar regions during the past 15 to 20 years. These sensors have suffered from a number of limitations. They have mostly operated in wavelengths hampered by the lack of daylight during the polar winter (visual) or by the presence of clouds (infrared). Recently passive microwave systems have been employed which overcome some of the above problems, but their resolution is poor (40 km). The use of an active microwave sensor such as synthetic aperture radar (SAR) appears to alleviate the spatial resolution problems. A synthetic aperture radar is an all weather, day or night active sensor capable of attaining high resolution (15 m) images of the earth's surface, oceans and cryosphere. The high resolution of SAR will no doubt shed new light on many of the processes and features of this ice-covered region.

1

Knowledge of the spatial extent and thickness of the sea ice canopy is important to those interested in operating in the polar regions, such as those involved in commercial shipping, mineral exploration, Naval operations and scientific endeavors. One of the major obstacles to observing or forecasting the spatial ice extent and thickness is the problem of identifying the distribution of the many different ice types. While SAR imagery of the polar regions will soon be available for scientific, commercial and military endeavors, our knowledge of how to use the data is lacking. One of the main challenges is to find a way to automatically provide maps of the spatial distribution of the different ice types in the polar regions. This is the topic of this study.

The primary objective of this study is to provide information that may be useful in designing an automated ice classification scheme with SAR data. Different ice types are clearly discernable in SAR images of the marginal ice zone. The challenge is to be able to develop an algorithm that will duplicate the skill of a human interpreter in classifying the various ice types. Past studies have shown that it is difficult to identify exactly what feature human interpreters use to distinguish between different ice types [Holmes et al., 1984; Trivedi et al., 1984]. One technique that has been used with moderate success focuses on the texture of the ice [Holmes et al., 1984; Trevedi et al., 1984]. The texture of different ice types is derived from the spatial variation of the backscatter intensity of SAR imagery. This concept of using texture to discriminate between various ice types will be compared and contrasted with the use of simple univariate statistics (mean, standard deviation, etc.) of the images to distinguish between the ice types. Within these two groups of statistics, texture and univariate, individual descriptor variables will be

2

analyzed using multivariate discriminant analysis and an optimal group of statistics demonstrating classification skill will be selected.

The data set used is from an experiment conducted in the marginal ice zone in April 1987. The data consist of SAR images of three different ice types (first-year, multiyear and odden) plus open water.

II. BACKGROUND

A. FUNDAMENTALS OF SAR THEORY

This section will review the fundamentals of SAR theory and the application of that theory to remote sensing of the polar regions. The frequency, flight geometry, and the high resolution of SAR imagery will be discussed.

1. Motivation for Synthetic Aperture Radar

Synthetic aperture radar is an all weather, day or night sensor capable of achieving high resolution images of the earth's surface. SAR operates in a range of electromagnetic wavelengths that are almost entirely unaffected by the earth's atmosphere. These characteristics make it an ideal sensor in the polar regions where the earth's surface is frequently obscured from space by clouds and darkness. The presence of water vapor between a satellite and the surface of the earth is the major factor interrupting continuous coverage of the earth's surface in the visible, infrared, and passive microwave wavelengths. Water vapor is present in the polar atmosphere in the form of clouds and fog. During the polar night (winter) sun angles are low or absent, thus restricting the use of the visible spectrum. SAR is not affected by atmospheric water vapor and is useful without sunlight because it is an active sensor.

2. Frequency Spectrum

The atmosphere has several electromagnetic (EM) transmission windows, i.e., regions of high transmittance of energy, that are useful for remote sensing. The

4

effectiveness of these windows is quantified by atmospheric transmittance. High values allow EM energy to pass through with minimal atmospheric interference. Figure 1 depicts the EM frequency spectrum and its associated transmission windows for the earth's atmosphere. SAR systems are designed to use transmission windows that fall in the 1 cm to 15 cm wavelength band. Table I shows the various radio frequency bands planned for use in space-born SAR platforms in the 1990's.
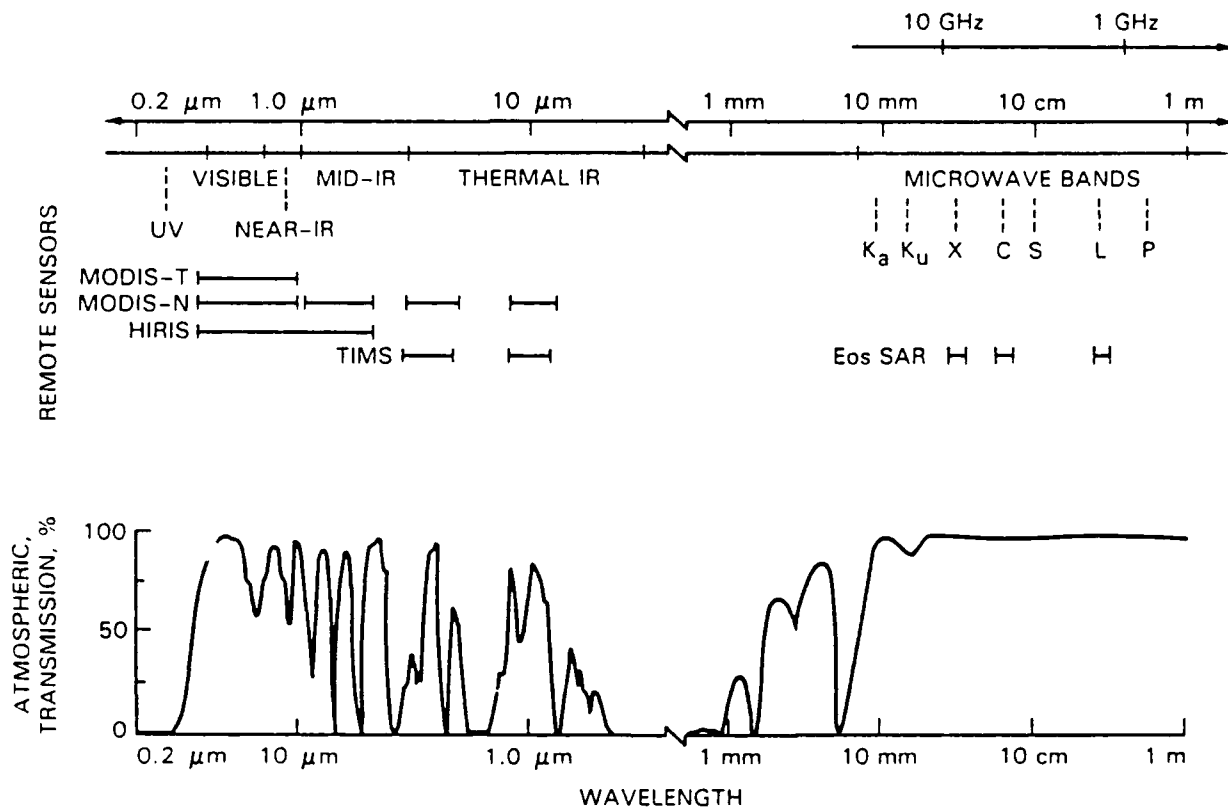
Figure 1. Transmission spectrum. Note high degree of transmittance in the centimeter wavelength [from SAR, 1987].

Table I. Future Planned Spaceborne SAR Platforms [from SAR, 1987].

Platform	ERS-1	JERS-1	RADARSAT	EOS
Country / launch date	European Space Agency / 1990	Japan / 1992	Canada /1993	United States / 1997
Frequency (GHz) [Band]	5.3 [C]	1.2 [L]	5.3 [C]	1.2 [L] 5.3 [C] 9.6 [X]
Resolution (m)	30 or 100	18	10-100	20-500
Swath Width (km)	80	75	50-500	30-700
Illum. Angle (Deg)	23	42	20-50	15-55

3. SAR Antenna Resolution

The SAR is capable of excellent range and azimuthal resolution because it uses short pulses (it is an active sensor) and satellite motion to synthesize an antenna much larger than the physical antenna size. Typically, the resolution of a sensor is given by $\lambda R/D$, where λ is the wavelength, R is the distance to the surface and D is the dimension of the antenna. For ordinary radars or passive microwave sensors operating from satellites this is nominally 10-50 km. SAR systems have a resolution on the order of 10 to 30 m.

6

a. Range resolution

SAR uses short pulses of EM energy to achieve its excellent range resolution. Figure 2 provides the defining geometry for SAR imaging. The range resolution of a radar(δ_y) is determined by the elevation angle (θ) of the radar, the pulse length (τ) and the speed of light (c).
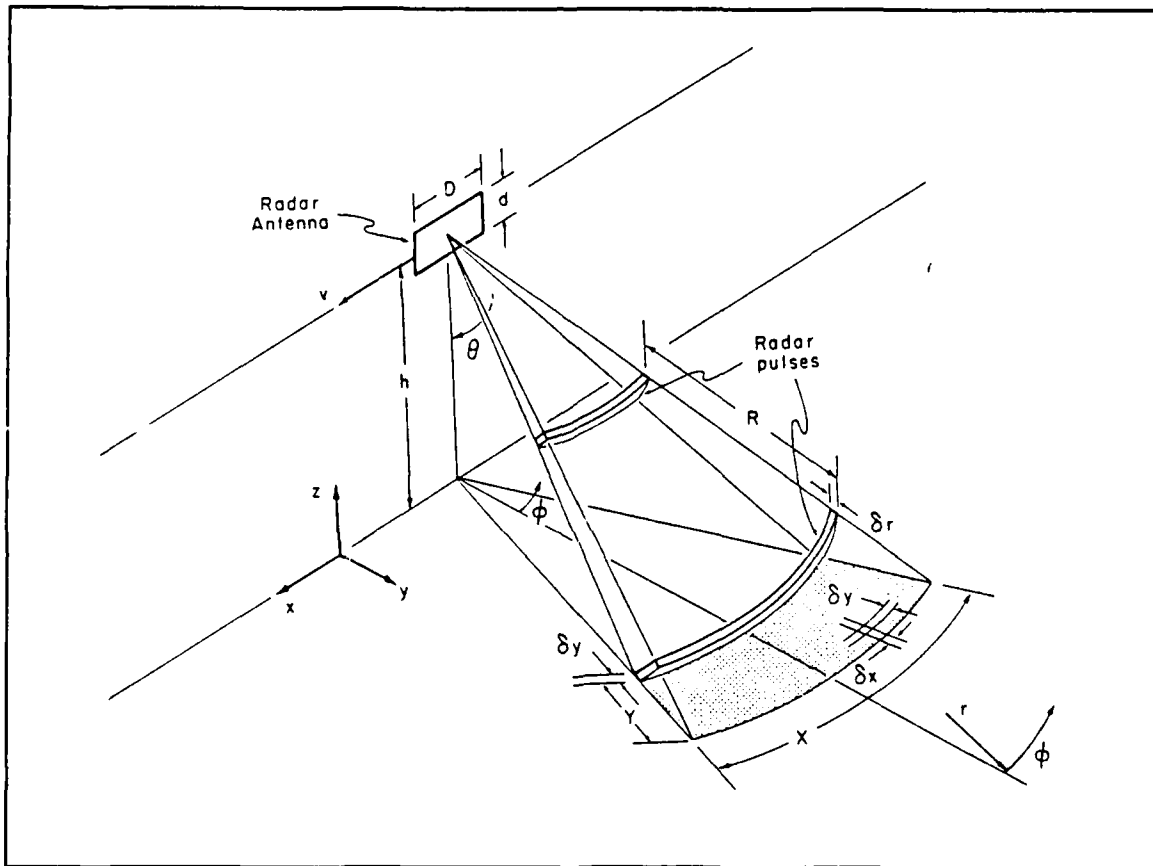
Figure 2 Fundamental SAR imaging geometry [from Stewart, 1985].

It is apparent from Equation (1) that the range resolution improves for shorter pulse lengths. A draw back of using short pulses is an inherent reduction in intensity. Pulse compression and frequency shifting techniques are used to maintain high

power and resolution. High power and short pulse lengths are desired for good range resolution. The time resolution of the return gives range resolution as with normal radar.

$$\delta_y = \frac{c\tau}{2}\sin\theta \qquad (1)$$

b. Azimuthal Resolution

The along-track resolution or azimuthal resolution depends upon the Doppler-shifted frequency of the return. Doppler shift is defined as:

> The change in frequency with which energy reaches a receiver when the receiver and the energy source are in motion relative to each other. [Glossary of Meteorology, 1986, p. 176]

The equation for the doppler-shifted frequency, f, is given by Equation (2)

$$f' = f_o \, (1 + \frac{V}{c}) \qquad (2)$$

where f_o is the original transmitted frequency and V the satellite velocity relative to an object on the earth's surface. For a SAR antenna, those points forward of a perpendicular to the direction of motion will be positively shifted and points aft of the perpendicular will be negatively shifted in frequency.

The onboard SAR receiver records the complex signal (amplitude and phase) of the returning radar pulse and transmits this information to a ground station. Post processing on the ground performs a complex convolution of many consecutive returns (looks) to sort out the doppler shifts from the reflecting surface. The effective

azimuthal or along-track resolution is given by: $\delta_x = D/2$, where D is the along-track dimension of the antenna. It appears that the along-track resolution is solely related to the antenna length with a shorter antenna providing better resolution. Swath width, however, is the restraining factor in determining the minimum antenna length [Stewart, 1985]. Swath width is defined as the width of the imaged area. Referring to Figure 2 the swath width is Y.

Resolution is often degraded to improve the signal to noise ratio. The more independent images the radar makes of a scene (looks), the clearer the image will become (this improves the signal to noise ratio). For example, a seven-look SAR will have less speckle (noise) than a four-look SAR [Stewart, 1985].

B.   ICE FORMATION AND MORPHOLOGY

This section will review the fundamentals of ice formation, forcing and features which influence EM interaction with sea ice. While a complete treatment of ice physics is well beyond the scope of this thesis, this section will summarily establish the link between ice age, salinity, temperature, density and surface roughness. Interested readers are referred to Bogorodoskii [1971], Timokhov [1974], Doronin [1977] and Untersteiner [1986], all excellent references on the physics of sea ice.

The polar ice cycle is driven almost entirely by the seasonal fluctuation of solar radiation. The polar winter consists of a total absence to a few hours of solar radiation wherein surface heat is lost to the atmosphere through net longwave radiation. The polar summer consists of long hours of daylight and high levels of short wave radiation. These

9

two dominant seasons, winter and summer, are separated by short transition seasons. The sea ice data used in this study (April 1987) is winter ice that has been imaged shortly before the transition to the summer regime.

Spatially the polar regions may be separated into four zones:

(1) The polar ice cap, a nearly continuous body of ice. (2) Landfast ice, which, as its name indicates, is frictionally anchored to the land and usually grounded on the continental shelf by pressure ridging. (3) A transition zone, a region of ice which is connected to the fast ice and extends to the pack ice and is a region of ice highly subject to frictional forcing. (4) The marginal ice zone, an area where the sea ice meets the open ocean. [Wadhams, 1986, p. 5]

The marginal ice zone is the primary area of interest for this study.

1. Sea Ice Formation

Sea ice formation is primarily a function of the vertical heat exchange across the air/ocean boundary. Its formation is predominantly influenced by the water temperature and salinity. The water temperature is primarily determined by the air temperature, evaporation, insolation and advection. The water salinity is affected by evaporation, ice formation and advection.

A vertical salinity gradient is normally present in sea ice. This vertical gradient exists primarily because of a vertical temperature gradient in the ice [Weeks and Ackley, 1982]. These gradients are shown in Figure 3. The presence of a vertical salinity gradient serves to complicate the modeling and understanding of EM ice interaction.

10

Figure 3. The vertical salinity gradient and its associated temperature gradient. Ordinate units cm. [from Campbell et al., 1975].
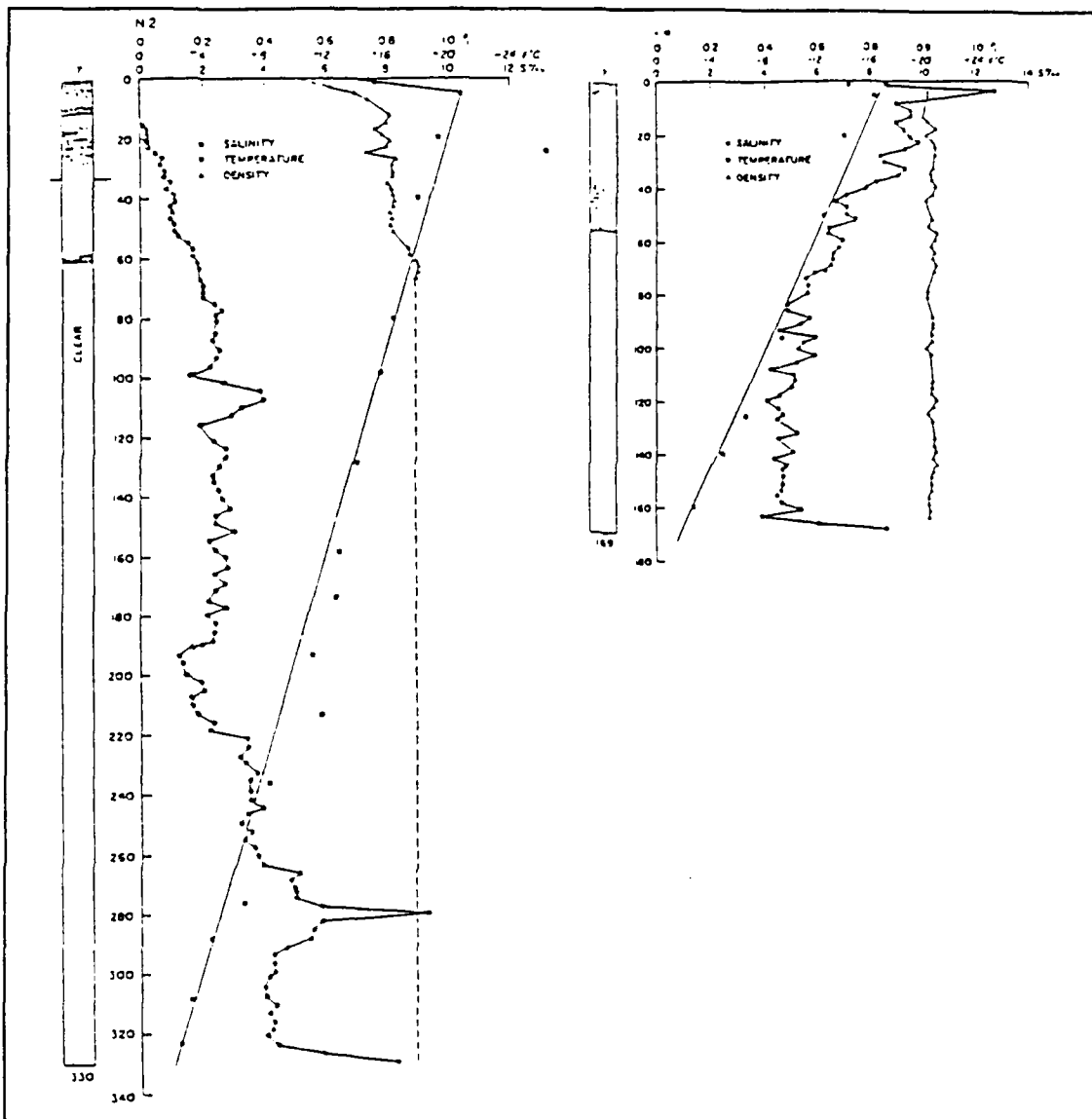
The age of ice affects its salinity content. As ice ages, brine pockets migrate downward towards the water interface due to gravity drainage and flushing [WMO, 1970]. Flushing occurs during the spring and summer thaw when water on the surface of the ice trickles down through the ice to the seawater ice interface. With increased warming, drainage channels form and the overall salinity of the ice decreases. Ice that has aged in

11

this manner and formed extensive drainage channels is known as rotten ice. This lower salinity ice will allow deeper penetration of the EM energy and consequently scatter from within the interior of the ice can occur. Scatter from the interior of the ice is known as volume scatter.

Ice thickness is of prime concern in polar operations. The varying thickness of sea ice is a function of its age and rate of formation. Sea ice may be found in thicknesses ranging from a few centimeters to a few meters. Generally, the older the ice, the thicker it is likely to be.

2. Ice Types Used In This Study

Three classes of ice are used in this study: new, first-year and multiyear. The age and thickness relationship of these three groups are the driving factors for establishing these ice categories.

a. New Ice

New ice is a general term applied to newly frozen sea ice. Its formal definition as provided by the World Meteorological Organization is:

A term for recently formed ice which includes frazil ice, grease ice, slush, and shuga. These types of ice are composed of ice crystals which are weakly frozen together (if at all) and have a definite form only while they are afloat.[WMO, 1970]

New ice can be found in many forms. The form that the new ice takes is largely a function of the wave and wind action. One of the forms that new ice may take is "nilas".

Nilas is a thin elastic crust of ice, easily bending in waves and swell and under pressure, thrusting in a pattern of interlocking "fingers". This ice has a matt surface and is up to 10 cm in thickness. [WMO, 1970]

12

With sufficient wave and wind forcing this ice type can form another type of new ice known as pancake.

Pancake ice is circular pieces of ice from 30 cm-3 m in diameter, up to about 10 cm in thickness, with raised rims due to the pieces striking against one another. It may be formed on a slight swell from grease ice, shuga or slush or as a result of breaking ice rind, nilas of under severe conditions of swell or waves, of gray ice. It also sometimes forms at some depth, at an interface between water bodies of different physical characteristics, from where it floats to the surface; its appearance may rapidly cover wide areas of water. [WMO, 1970]

A special form of new ice which exhibits rapid regional growth and retreat is odden.

The "Odden" is an extensive protuberance of sea ice in the Greenland Sea Basin that extends several hundred kilometers into the Greenland Sea. The basin circulation in the Greenland Sea is characterized by the cyclonic circulation in the Boreas and Greenland Basin. These two areas are also known to show large fluctuations in the ice cover. The rapid 2-4 day oscillations of this zonal ice edge extent centered at 74°N appears to be a near annual event normally first encountered at the beginning of the winter season. [Sutherland and Shuchman, 1989, p. 1539]

Sutherland and Shuchman suggest that off-ice edge winds with air temperatures of -10° to -20° C for two to three days is sufficient for the formation of this ice type. Regardless of it's formation mechanism, the important fact is that odden is a special category of new ice comprised of nilas 3-5 cm thick, transitioning into 5-10 cm pancake flows [Sutherland and Shuchman, 1989]. Because odden is similar in appearance to new ice, one might expect that the results of analyzing the texture features of odden can be applied to new ice found in other regions of the arctic.

b.   First-year ice

First-year ice is, as it's name suggests, ice of not more than one year's growth. It develops from new ice and ranges in thickness from 30 cm to 2 m [WMO,

1970]. It may be subdivided into thin first-year ice and thick first-year ice. First-year ice is typically lower in salinity than new ice because the entrapped brine has begun to migrate toward the ice-water interface. Convergent forcing of first-year ice sheets by wind and/or water motion develop pressure ridges. Significant change in the surface appearance of first-year ice is thus likely.

c. *Multiyear Ice*

Multiyear ice is the oldest and thickest ice found in the Arctic. This is sea ice which has survived at least one summer's melt cycle. Multiyear ice ranges in thickness from 2 m to 4 m based on it's age and location within the Arctic basin. It is usually visually blue due to refreezing of fresh water in the brine drainage channels which in time become well developed [WMO, 1970]. The salinity of multiyear ice is the lowest of the various ice types. This low salinity will allow penetration of EM energy into the ice with subsequent volume scattering occurring.

3. Ice Texture Features

As a result of weathering and forcing by wind, currents and tides, the various ice forms develop distinct surface features or textures which can be used as classification aids. It is a primary goal of this analysis to be able to use these distinct features as imaged by SAR to classify the ice into three thickness categories: new(< 0.5 cm), first-year (0.5 m), and multiyear (2-4 m). To accomplish this SAR must rely heavily on the radar signature of the surface of the ice [Ketchum, 1981]. The radar signature depends on the previously mentioned ice characteristics (salinity, density, thickness) as well as the

14

spatial variation of the surface roughness. Proper identification of these surface roughness features are an important aspect in the correct classification of various sea ice types. The two main parameters influencing the return of EM energy to the SAR antenna are surface reflection and volume scatter as depicted in Figure 4. Although this drawing is for glacial ice, the principal scattering types pertain to sea ice as well.
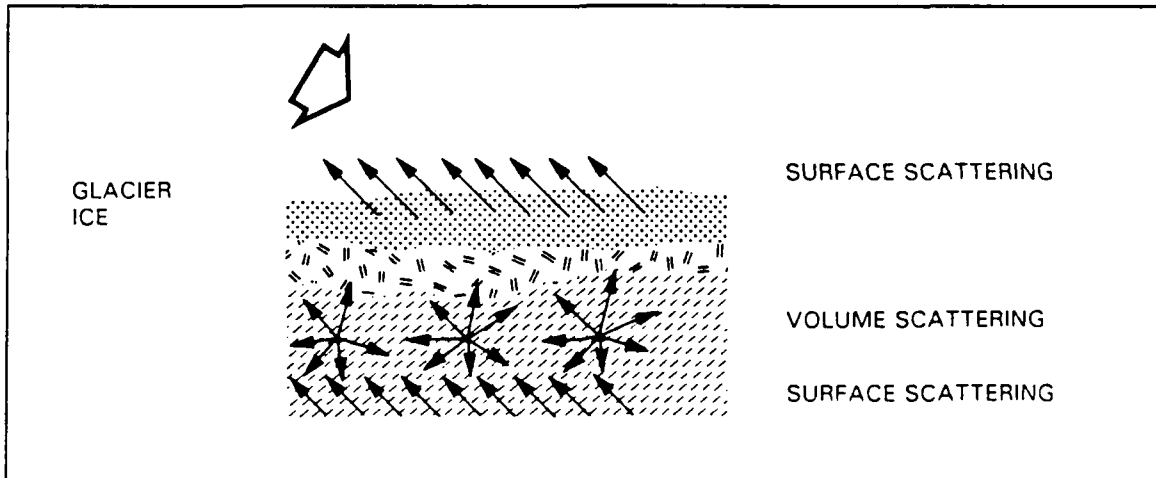
Figure 4. Scattering types [from SAR, 1987].

a. *New Ice Texture*

New ice will usually be smooth because the ice has no strength, i.e., it does not yet act as a plate or sheet. New ice will deform with the ocean surface. When imaged with SAR, new ice may appear very similar to the sea surface when unruffled by wind waves. New ice types and older non-ridged first season ice generally experience less deformation than older forms. They usually have smoother surfaces and hence are found to produce less radar backscatter [Ketchum, 1981].

As the new ice begins to thicken, it frequently forms pancake ice with it's characteristic upturned edges. The upturned edges provide a good radar cross-section to return EM energy to the SAR. Odden ice frequently appears in this pancake form.

b. First-year Ice Texture

As new ice begins to form a consolidated sheet, it transitions into thin first-year ice. Thin first-year ice begins to become rigid enough so that divergent, convergent, and sheer stresses begin to leave their mark on the surface texture of the ice. As the ice increases in thickness throughout the winter, the ice sheets become more rigid and may eventually form ridges. Pressure ridges with heights of 8-10 m are occasionally seen in the Arctic although the majority are considerably smaller [Pounder, 1965].

c. Multiyear Ice Texture

The surface of multiyear ice is often found to have hummocks or large mounds on the ice which have been rounded due to weathering and are visually smoother than first-year ice. However, in the cm wavelength bands, where EM energy penetrates into the ice, internal discontinuities influence the backscatter return. EM energy can penetrate into multiyear ice because of it's lower salinity. For this reason the texture of the multiyear ice will appear rough and bright in the centimeter wavelength band. It has been found by Ketchum [1981] that older ice forms experience more deformation than younger ice. However, older ice generally has a smoother surface appearance due to weathering which has removed the angular features of first-year ice. Older pressure

16

ridges are somewhat smoother especially those blanketed with snow. Therefore, volume backscatter vice reflection is the dominant feature for this ice type.

C.   ICE AND EM RADIATION INTERACTION

The main factors influencing the imaging of a scene are the illumination of the scene, the reflectance of the surfaces and the imaging geometry of the sensor. The illumination of the scene by the SAR is fixed (or calibrated in some relative sense). The geometry has been described in Figure 2. This section will focus on the reflectance of the imaged ice surfaces. The variation in the near-surface salinity and the surface roughness of the sea ice are the main factors affecting the interaction of EM radiation with sea ice.

1.   EM Properties of Ice

The electromagnetic properties of sea ice are primarily controlled by the temperature and salinity of the ice in that both affect the complex dielectric constant. The complex dielectric constant defined as $\varepsilon = \varepsilon' + j\varepsilon''$ is comprised of two parts, the real part, ε' and the imaginary part, ε''. The complex dielectric constant quantifies the response of a material, ice and water in this case, when an EM field is induced (the incoming radar beam). This constant provides a measure of how strongly the polarized ions or molecules will align themselves with a EM field. Ice, because of its rigid molecular structure, interacts weakly with an EM field and thus has a low dielectric constant. Water molecules, however, are strongly polarized and are free to move to interact with an EM field, thus increasing the dielectric constant. [Lewis et al., 1987]

17

The imaginary portion of the complex dielectric constant, also known as the dielectric loss, determines the depth to which EM energy will penetrate into the ice [Weeks and Ackley, 1982]. The depth at which the EM energy reaches e^{-1} of it's value at the surface is known as the skin depth. The skin depth will prove to be an important parameter in distinguishing old multiyear ice (ice of very low salinity) from new first-year ice (ice of substantially higher salinity). As stated previously, in multiyear ice the EM radiation interacts by volume scatter from cracks and bubbles within the ice. For younger first-year ice surface scatter dominates. This difference in penetration of EM energy in sea ice can be described by the relative variation of the skin depth of the ice.

Much work has been conducted to determine the effect of the ice salinity and temperature on the dielectric loss. Generally it has been found that the temperature and salinity are both directly correlated with the dielectric loss [Weeks and Ackley, 1982]. This temperature, salinity, dielectric relationship may be seen in Figure 5. Note that as the salinity increases, the dielectric loss increases.

The real part of the complex dielectric constant (ϵ') quantifies the ability of the ice to reflect the EM energy. With a knowledge of the relationship between temperature, salinity and the dielectric constant, it is possible to clearly identify the major ice types on a graph of the dielectric constant. Figure 6 shows the temperature relationship with the dielectric constant for the major ice types used in this study. Note that frazil ice (similar to odden) has the highest dielectric constant followed by first-year and lastly multiyear ice. Also, note that each ice type exhibits a decreasing dielectric constant with decreasing temperature.
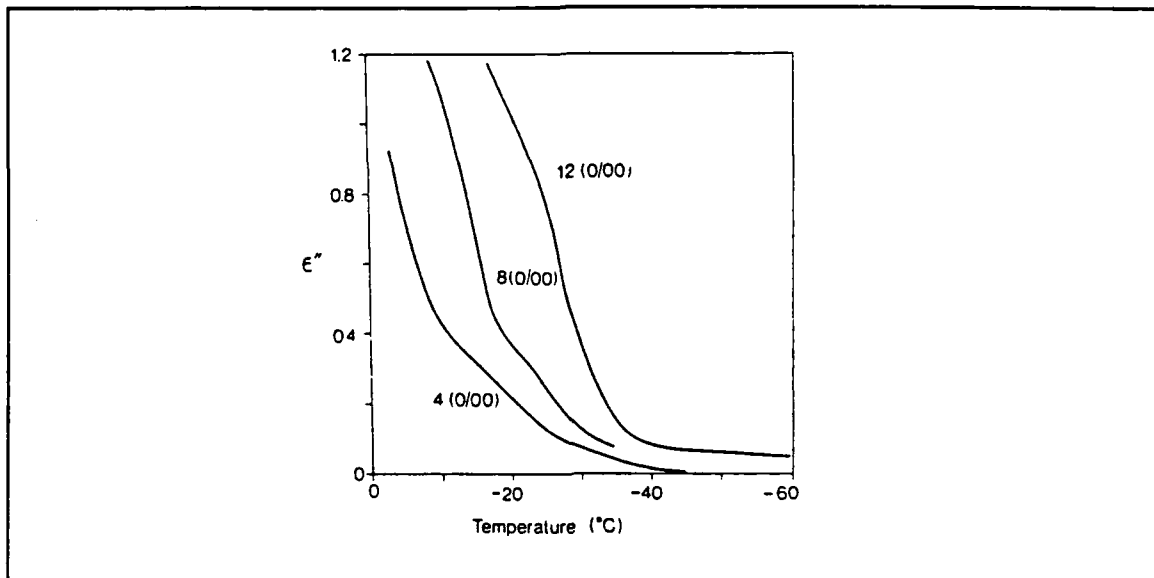
Figure 5. Dielectric loss versus temperature for several salinities of sea ice. Note that as the temperature and salinity decrease, the dielectric loss also decreases [from Hoekstra and Spanogle, 1972].

The ice density affects the interaction of EM energy with the ice. The lower density and lower dielectric constant of older ice forms allows the radar to volume scatter from the interior of the ice. Figure 7 graphically depicts this volume scatter and the different scattering types that may be found in using active microwave signals to image ice.

2. Surface Roughness and Radar Cross-section

The surface roughness of polar ice is important in providing a variation in the backscatter intensity from SAR. The backscatter intensity is proportional to the radar cross-section. Radar cross-section may be defined as the strength of a radar target expressed in terms of the cross-section of an ideal reflector which would give the same returned signal strength. As the ice surface becomes rougher, the radar cross-section

19
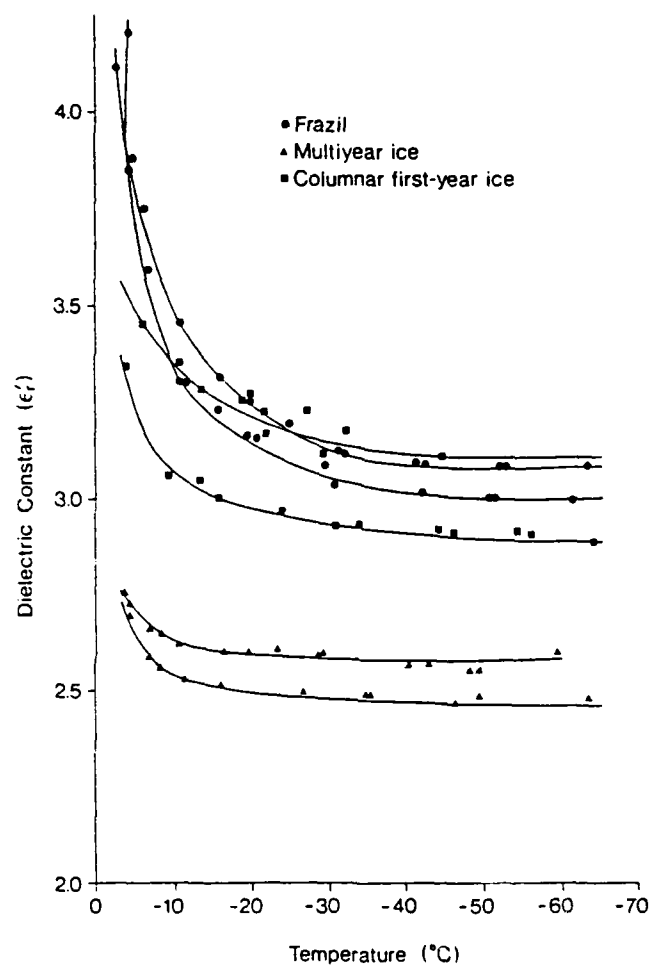
Figure 6. Dielectric constant versus temperature for sea ice [from Vant et al., 1974].
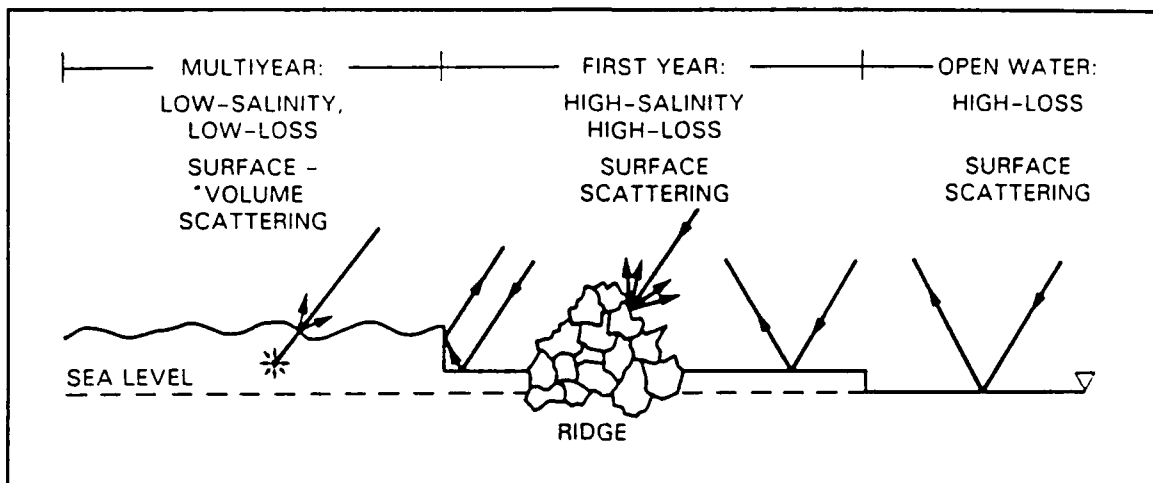
Figure 7. Interactions between radar and different ice types. The increase in salinity decreases the skin depth thus preventing deep penetration of the EM radiation [from SAR, 1987].

presented to the SAR increases and a greater probability exists that individual facets of the ice will be perpendicular to the incoming radar beam. The fact that the backscatter cross-section presented by open water, first-year, odden and multiyear ice increases, respectively, in magnitude can be explained solely by surface roughness considerations [Ketchum, 1981]. The ice surface roughness will vary because of its formation mechanics. Open water in a low wind environment will have a flat surface with little radar cross-section. First-year ice may also have a relatively flat surface with some surface roughness (ridges) due to shearing and compressional stress. Odden, which is a specific variety of new ice, appears rough due to the upturned edges of pancake-like ice. Multiyear ice has undergone numerous dynamic forcing events and is likely to have a surface with pressure ridges and ice rubble on the surface. In addition to the surface roughness, the multiyear ice radar cross-section is enhanced by volume scatter due to its lower salinity and lower density.

It should be clear that the interaction of EM energy with sea ice is complex. The EM interaction depends largely on the dielectric constant and the surface roughness. This study is based on the hypothesis that sufficient differences exist in the backscatter characteristics of the various sea ice types and open water for SAR to be an effective ice classification tool. Different samples of an ice type may have different properties based on the dielectric properties and surface roughness of the samples. The natural variation in the ice characteristics mean that not all ice from one category will have the same radar return. It is this variation that complicates the classification of ice using SAR.

D. ICE CLASSIFICATION BACKGROUND

This section will review several ice classification methods that have been used by other researchers and introduce the method chosen for this investigation. The challenge of using SAR to classify polar ice types is in developing an automated algorithm that will, in real-time or near real-time, accurately classify the various ice types that have been imaged. Many approaches have been attempted to accomplish this classification with active EM sensors.

Early attempts to classify ice types in the 1960's focused on finding a particular physical property such as the dielectric constant, salinity or surface roughness that was directly measurable by using radar. Researchers began to focus on the varying textures or surface features to which radar back-scatter was sensitive. Anderson [1966], Moore [1966] and Rouse [1969] did some of the early work in using a scatterometer as a remote

22

sensor to determine the surface roughness of polar ice. This work began to point the way towards inferring gross ice thickness based on scattering coefficients.

Side looking air-borne radar (SLAR) was developed for military use and took advantage of the microwave region of the EM spectrum. This radar is termed 'side-looking' because it transmits a beam in a fixed direction perpendicular to the line of flight [Johnson and Farmer, 1971]. Anderson [1966] showed that a SLAR system could effectively image large areas of sea ice. In a navigational experiment with the S.S. *Manhattan*, the use of a SLAR to identify and aid in safe, efficient navigation through polar ice was demonstrated [Johnson and Farmer, 1971]. The interpretation of the ice types imaged with this SLAR was performed by highly trained ice observers. The important results of this experiment were that radar images can assist in the safe transit and operations in and through polar ice and that human interpretation of radar ice images is extremely subjective [Johnson and Farmer, 1971].

During the early 1970's researchers began searching for a way to use the modern computer to reproduce the human's ability to discriminate between different images. Haralick et al., [1973] focused on the use of texture to identify objects or regions of interest in an image. Most people have some concept of texture but a clear definition has been illusive. Webster's dictionary [1984, p. 1220] defines texture as "something composed of closely interwoven elements" or "the disposition or manner of union of the particles of a body or substance." Haralick et al., [1973] provide one of the best definitions of texture as used in image processing applications. Their paper highlights the features that humans use to interpret pictorial information.

Spectral, textural and contextual features are the three fundamental pattern elements used in human interpretation of color photographs. Spectral features describe the average tonal variations in different bands of an EM spectrum, whereas textural features contain information about the spatial distribution of tonal variations within a band. Contextual features contain information derived from blocks of pictorial data surrounding the area being analyzed. When small image areas from black and white photographs are independently processed by a machine, then texture and tone are most important. [Haralick et al., 1973, p. 610]

They go on to highlight the fact that tone refers to the variation in shades of gray from white to black. The range of tone is fixed by either the imaging or display system dynamic response while texture is limited by the SAR processing resolution. The spatial distribution of the tonal elements in an image are the way humans perceive texture. The tonal - textural relationship is the key concept to understand when working with texture statistics. The tone of an image is represented by the shades of gray from black to white. These gray shades are represented digitally in a computer image as an integer value in a spatial grid. It is the spatial variation in these gray shades that allows the texture of a surface to be analyzed. One would expect greater spatial tonal variation to be found over a rough surface and lowest spatial variation over a smooth surface. Many different attempts to discern the texture of an image have been made with varying degrees of success. Some of the methods attempted to discern the texture are reviewed below.

1. **Fourier methods - Power Spectral Method (PSM)**

The PSM involves taking the Fourier transform of an image and analyzing the frequency spectrum of the gray shades. Different textures show quite distinct frequency spectra. A key theoretical study of texture algorithms performed by Connors and Harlow [1980] showed the relative merits of the PSM compared to the spatial gray level

24

dependence method (SGLDM, referred to in this study as gray level co-occurrence GLC matrices), the gray level run length method (GLRLM), and the gray level difference method (GLDM). These three methods will be described in more detail below. Their study showed the PSM to rank last in ability to discriminate textures known as Markov chains. This approach has been discarded as a result of this theoretical study. An experimental study performed by Weszka, Dyer and Rosenfield [1976] on actual textures supports this decision.

2. Autocorrelation Methods

Some attempts have been made to quantify "coarseness" by using autocorrelation techniques. The coarseness of a pattern has been proposed to be measured by the rate at which its autocorrelation function drops from its peak value with a faster drop-off implying a coarser texture. The coarseness is defined by its e-folding value or displacement when the autocorrelation is reduced to $(e)^{-1}$ of its peak value [Rosenfield, 1975]. These results demonstrated that the autocorrelation function could capture the texture of an image as perceived by human interpreters. Later work showed that distinct texture patterns could be developed that were not discernable with the autocorrelation technique [Connors and Harlow, 1980]. In addition to being computationally expensive, autocorrelation techniques have a problem with edge effects. Rosenfield [1975], Connors and Harlow [1980], and others have found that autocorrelation and Fourier-based features perform more poorly than statistical features. For this reason most of the texture work performed in the last ten years has involved some form of statistical texture measure.

3. Statistical: Gray-Level Run Length Method (GLRLM), Gray-Level Difference Method (GLDM)

These two methods of analyzing images have also been tried with limited success. The GLRLM method counts the number of pixels that share the same gray shade along some direction in the image. A GLRLM matrix is computed for various angles in an image. The entries in the matrices are indicated by how long a run of length can be made for each gray shade in a image. This is computed for a number of different

26

angles in the image. Connors and Harlow [1980] found that it was easy to generate visually distinct textures that could not be discriminated using the GLRLM.

The GLDM is based on the difference in the gray shades along some vector of length. The gray level value of the pixel at the origin of the vector is subtracted from the value of the pixel at the termination of the vector. Ultimately, probability density functions and texture measures are computed. Connors and Harlow [1980] also found the GLDM was not as skillful as the GLC matrices in classifying actual textures.

4. Gray Level Co-Occurrence (GLC) Matrices

Since the early 1980's most researchers have concentrated on using the gray level co-occurrence matrix to analyze textures in an image. Various researchers have found that the GLC matrix captures the texture in an image most closely matching a human's ability to perceive texture [Haralick, 1973; Weszka et al., 1976; Shanmugan et al., 1981].

> The GLC matrices provide a basis for the global analysis of textured objects due to several reasons. These include the fact that GLC matrices have been used successfully on a number of textured object analysis problems. These matrices are known to contain enough texture-context information to match a level of human texture perception. Further, a comparison study has shown them to contain more important texture-context information than the intermediate matrices of a number of other texture algorithms (Connors and Harlow,1980). Finally, it is known that these matrices can be used to gauge useful structural information in the global analysis of texture. [Trivedi et al., 1984, p. 202]

Trivedi et al. [1984] indicate that the spatial gray level dependence method (SGLDM) or GLC matrix is the method of choice for texture analysis. The GLC matrix is based on the second-order joint conditional probability density function, $f(i,j \mid \Phi(d,\theta))$; where $\Phi(d,\theta)$ is a vector of length d and θ is an angle measured from the vertical or column elements

27

in an image. The $f(i,j \mid \Phi(d,\theta))$ represents the probability of finding gray levels, i and j, at the base and termination points of a vector $\Phi(d,\theta)$. This GLC matrix is often written as $S_\theta(d)$ with individual elements of the matrix written as $s_{\theta(i,j \mid d)}$. Because a digital image provides discrete pixel values, choices of angle θ and length d for this vector Φ are limited. Additionally, Connors and Harlow [1980] point out that

$$S_{0^\circ}(d) = S_{180^\circ}(d)'$$

$$S_{90^\circ}(d) = S_{270^\circ}(d)', \text{ etc.....}$$

Where $S_\theta(d)'$ is the transpose of the matrix.

Therefore no new information is gained by computing GLC matrices for any angles other than 0° to 180° (or conversely 180° to 360°) [Connors and Harlow, 1980]. Once the GLC is computed, statistical descriptors of this "texture" space are computed. These texture descriptors are chosen to capture and describe the variation in gray levels from the image domain.

a.   Texture Statistics

It is a widely held view that texture statistics can successfully separate various ice types. One of the first attempts to use texture statistics derived from the GLC matrix in a real-time fashion was carried out by Holmes, Nüesch and Shuchman [1984]. In their work, great strides were made towards developing a digital procedure for identifying ice types in SAR imagery and adapting it to real-time processing of digital image data. Texture statistics as defined by Connors and Harlow [1980] are a group of first and second order statistics that may be derived from a GLC matrix and which capture the spectral textural and contextual variations referred to by Haralick et al. [1973].

It is the goal of texture analysis to be able to use texture statistics to quantify these spatial variations.

Equations (3)-(8) have been suggested for use in quantifying texture [Connors and Harlow, 1980; Trivedi et al., 1984]. Exactly what texture feature is captured by each statistic is still somewhat unclear. Shokr [1989] suggests that high inertia values mean higher contrast texture while uniformity (energy) is mainly influenced by high-value entries of the matrix.

Uniformity as the name indicates can be considered as a measure of the homogeneity of gray level distribution. A high uniformity value means more homogeneous region and vice versa. Entropy, as pertaining to the random process theory, is a statistical measure which is used to quantify the disorder in a function. [Shokr, 1989, p. 765]

The important point is that each of these statistics describe either the rate at which gray shades change in a GLC matrix or the degree of randomness in the GLC. This, in turn, hopefully, describes some fundamental feature of the ice. It is the combination of these statistics in a manner which will allow discrimination of different textures that forms an effective texture classifier.

$$Energy = \sum_{i=0}^{N_G-1} \sum_{j=0}^{N_G-1} \left[s_\theta(i,j|d) \right]^2 \qquad (3)$$

$$Correlation = \frac{\sum_{i=0}^{N_G-1} \sum_{j=0}^{N_G-1} (i-\mu_x)(j-\mu_y)s_\theta(i,j\,|\,d)}{\sigma_x\sigma_y} \qquad (4)$$

$$Inertia = \sum_{i=0}^{N_G-1} \sum_{j=0}^{N_G-1} (i-j)^2 s_\theta(i,j\,|\,d) \qquad (5)$$

$$\begin{matrix}Cluster\\prominance\end{matrix} = \sum_{i=0}^{N_G-1} \sum_{j=0}^{N_G-1} (i-j-\mu_x-\mu_y)^4 s_\theta(i,j\,|\,d) \qquad (6)$$

$$\begin{matrix}Local\\homogeneity\end{matrix} = \sum_{i=0}^{N_G-1} \sum_{j=0}^{N_G-1} \frac{1}{1+(i-j)^2} s_\theta(i,j\,|\,d) \qquad (7)$$

$$Entropy = -\sum_{i=0}^{N_G-1} \sum_{j=0}^{N_G-1} s_\theta(i,j\,|\,d)\log s_\theta(i,j\,|\,d) \qquad (8)$$

In these equations $s_\theta(i,j\,|\,d)$ is the (i,j)th element of $S_\theta(i,j\,|\,d)$, the GLC matrix for a particular angle or combination of angles. N_G are the number of gray levels in the raw image and μ_x, μ_y, σ_x, σ_y, are the respective mean and standard deviations for the rows

and columns of the image.   Each of the texture statistics selected above attempt to capture a unique feature of the texture so that the expected value of each statistical texture descriptor will be unique.   Figure 8 provides an excellent presentation of the steps involved in defining a texture analysis system.

```
        ┌─────────────────────┐
        │   DIGITAL IMAGE     │
        │ (PICTURE FUNCTION g)│
        └─────────────────────┘
                  ▼
        ┌─────────────────────┐
        │   INTERMEDIATE      │
        │  MATRICES OF THE    │
        │  TEXTURE ALGORITHM  │
        └─────────────────────┘
                  ▼
        ┌─────────────────────┐
        │     VECTOR OF        │
        │     MEASURES         │
        └─────────────────────┘
                  ▼
        ┌─────────────────────┐
        │      PATTERN         │
        │     CLASSIFIER       │
        └─────────────────────┘
```
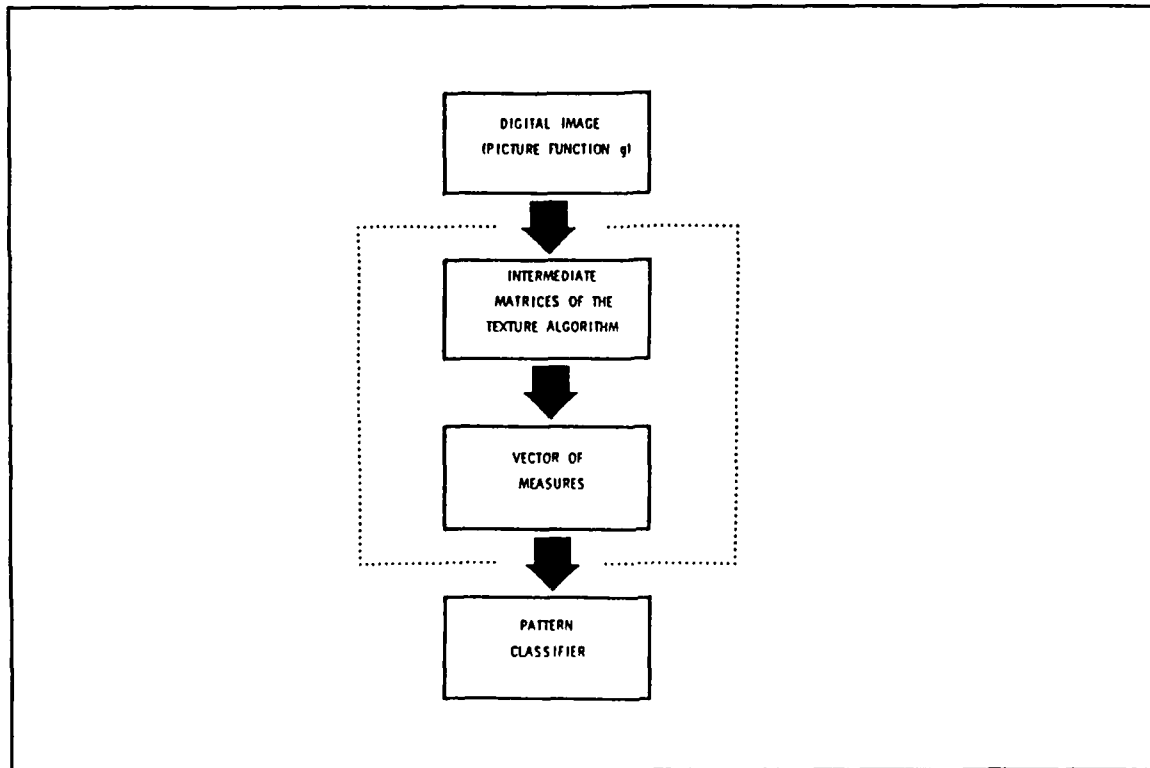
Figure 8. Texture classification steps. The flow diagram depicts the steps to using texture statistics to classify texture [from Connors and Harlow, 1980].

31

b. Texture Image Scale

Texture image scale addresses the issue of how big or small the texture features are in an image. When designing an optimal texture algorithm, two questions must be answered: 1) For a given texture, what image area sub-sample will have the maximum likelihood of containing only one texture? 2) Within an image area sub-sample, what is the size of the texture element that is to be captured?

To answer the first question one must have some prior knowledge of the scene being analyzed. A given scene may be made up of a number of textures. To create a GLC matrix that only contains one texture it is necessary to sub-sample the image. Selection of the correct image sub-sample area is controlled by what might be called a macro texture. Ideally a sub-sample of the image contains only one texture $X_1(n,m)$, such that it is discernable from any other texture, $X_n(n,m)$. Some work has been done on what is known as a global approach to texture analysis in which the question of sub-image sampling is approached using linear unmixing to determine how many different textures a sub-image may contain [Holyer, 1989]. This global approach sacrifices some spatial certainty for accurate texture classification.

To answer the question of texture element size an investigator is concerned with what is called micro texture or how small the texture features are. The selection of a vector length, d, should be able to capture the texture in a sub-image sample. If d is too large, important variations in tone may be missed in generating the GLC matrix. The upper bound on the length of d is the number of pixels in a texture sub-image. The lower bound on d is 2 pixels. The optimal vector length may lie

32

somewhere between the two bounds. It is recognized that selection of the correct vector length is problematic [He and Wang, 1989]. Ideally, one should know a priori on what scale the texture in an image varies and select a vector length to capture the micro scale texture. The approach used in this study assumes a continuous or pure texture for each image being analyzed.

c. Texture Directionality

GLC matrices are directionally sensitive to texture features. A GLC matrix generated with one particular vector $\Phi(d,\theta_1)$ may contain information not found in a GLC matrix generated using another $\Phi(d,\theta_2)$. In most cases a non-direction biased GLC matrix is desired. However, actual images are usually randomly oriented. Numerous approaches to developing texture measures that are not directionally biased have been suggested. Holmes et al. [1984] and Shokr [1989], for example, average their GLC matrices over four different angles (0°, 45°, 90° and 135°). He and Wang [1989] provide a variation on the generation of non-directional GLC matrices by using a "texture unit". Their "texture unit" assigns a texture value to each pixel in an image based on the relative intensity of neighboring pixels. This approach has not been used extensively and appears computationally expensive and will not be used in this study.

5. Statistical Descriptors

The statistical descriptors used in this work are composed of texture statistics and univariate statistics. The six texture descriptors are discussed in the previous section. Texture statistics have been pursued for image classification because numerous theoretical

examples have demonstrated the failure of univariate statistics to be able to differentiate between two images that are visually distinct. However, this study will use both univariate and texture statistics to allow for a relative comparison of their strengths in discriminating between different ice types. The univariate statistics used in this work to discriminate between various ice types are standard first and second order statistical functions. They are mathematically defined by Equations (9)-(15).

a. Univariate statistics

Univariate statistics are the most commonly used group of statistics used to describe the distribution of data. The most frequently used are the mean, range, standard deviation, skewness, kurtosis, coefficient of variation. They are mathematically defined as:

$$Mean = \bar{x}_w = \frac{\sum f_i w_i x_i}{\sum f_i w_i} \qquad (9)$$

$$Standard\ deviation = s_w = \sqrt{\frac{\sum f_i w_i (x_i - \bar{x}_w)^2}{n-1}} \qquad (10)$$

$$Variance = s_w^2 = \frac{\sum f_i w_i (x_i - \bar{x}_w)^2}{n-1} \qquad (11)$$

34

$$Skewness = \frac{\dfrac{\sum f_i w_i (x_i - \bar{x}_w)^3}{n}}{\left[\dfrac{\sum f_i w_i (x_i - \bar{x}_w)^2}{n}\right]^{3/2}} \qquad (12)$$

$$Kurtosis = \frac{\dfrac{\sum f_i w_i (x_i - \bar{x}_w)^4}{n}}{\left[\dfrac{\sum f_i w_i (x_i - \bar{x}_w)^2}{n}\right]^2} - 3 \qquad (13)$$

$$Range = x_{max} - x_{min} \qquad (14)$$

$$\begin{matrix} Coefficient \\ of\ variation \end{matrix} = \frac{s_w}{\bar{x}_w} \qquad (15)$$

Where: x_i = the intensity of one pixel in the image,

$\bar{x}$ = the mean value of x

f_i = the frequency

w_i = a weighting coefficient

35

These univariate statistics, derived from the original gray shade images, together with texture statistics, derived from the GLC matrices, will be used to discriminate between three groups of ice and water in this study.

Univariate statistics have been shown to be unable to successfully discriminate between two visually distinct images. A excellent example of the failure of univariate statistics was provided by Trivedi et al. [1984]. Figure 9 shows that both the "T" and "L" have the same univariate statistics. These two images can be differentiated with the use of GLC matrices and texture statistics. While this example and many others like it appear to be important for the discrimination of man made objects, recent work indicates that univariate statistics do a good job in differentiating between different ice types [Shuchman et al.,1989; Shokr, 1989].
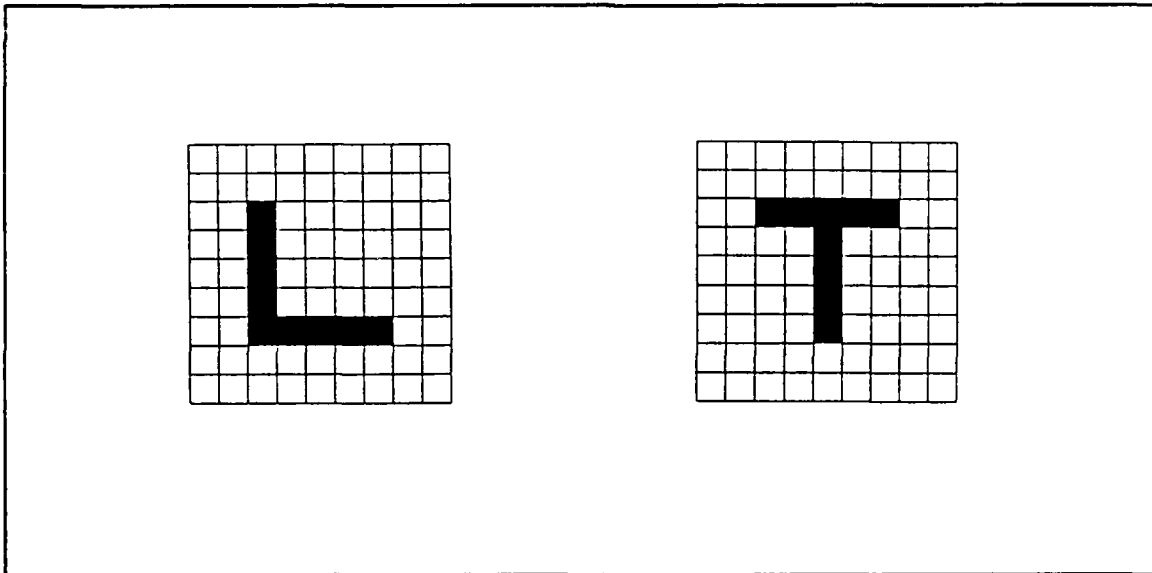
Figure 9. Example of the failure of univariate statistics to be able to differentiate between two visually distinct objects. The two letters have the same grey level histogram [from Trivedi et al., 1984].

36

6.   Variable Optimization

Two major analysis tools have been developed to identify which statistical descriptors best classify groups of ice and water: principal component analysis and discriminant analysis. Both methods are a type of eigenvector analysis and operate on a co-variance or correlation matrix.

a.   Principal Components

The method of principal components is a multivariate technique which combines highly correlated variables together to form factors which describe a basic principal or characteristic of a group [Kachigan, 1982]. The goal of principal component analysis is to simplify the description of a set of interrelated variables. Principal components are commonly used in the exploratory phases of a investigation to attempt to uncover which descriptor variables are most important in their contributions to a desired factor. Kachigan [1982] provides an excellent graphic example of factor analysis (Figure 10). In this figure the descriptor variables, V_1, V_2,.....V_9, are clustered in three groups. Each of these three groups reflect an underlying factor. The principal component analysis reduces the number of descriptor variables to three factors. As pointed out by Kachigan [1982], this textbook example is clear cut compared to real world problems. In most research problems the descriptor variables in each of the groups, V_1,...V_{1n}, V_2,...V_{2n}, and V_3,...V_{3n}, will have some overlap. Principal component analysis will provide factors that are independent of each other and then these factors can be used to form an eigen basis for the data [Kacihgan, 1982]. The combination of a set of descriptor variables such as Equations (3)-(15) to form factors may assist a researcher in uncovering
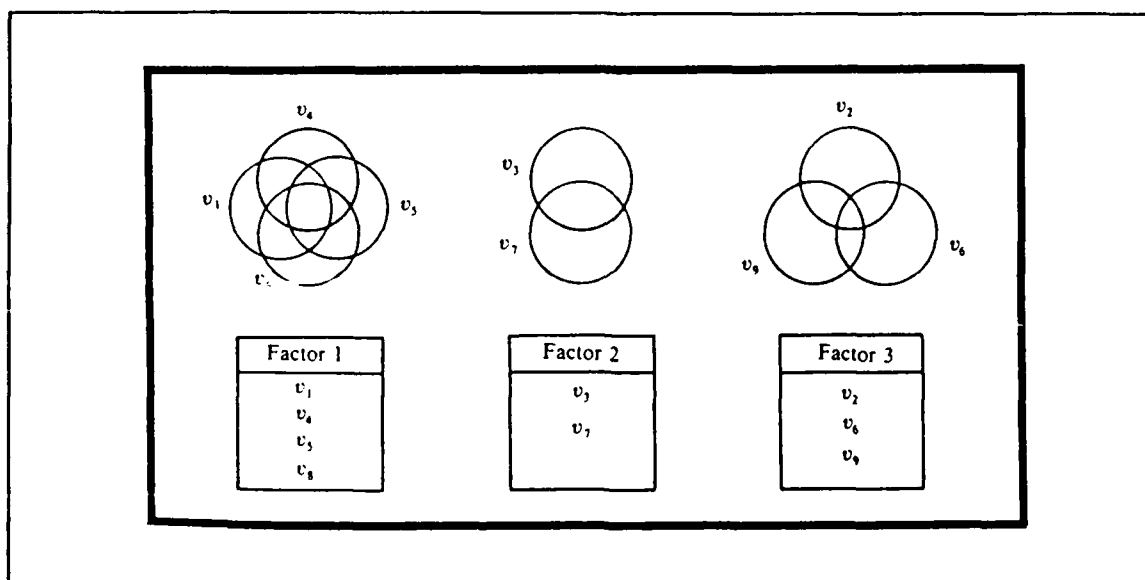
Figure 10. Venn diagram depicting the clustering of variables having a common underlying factor. Factor analysis will find the factor by analysis of a correlation matrix [from Kachigan, 1982].

common traits in a data set.

Principal component analysis is used to simplify a data set and gain insight, screen variables for use in statistical investigations, and summarize the data, sample and cluster variables. Frequently principal components are used to isolate factors for use in a discriminant analysis. Principal components were not used to reduce the dimensionality of the data set in this study. This thesis attempted to use principal component analysis to try to identify characteristics for each group of ice or open water. Unfortunately, because of the difficulty in interpreting the factors, this approach was abandoned. When the individual texture descriptors are better understood, principal component analysis may provide some useful information.

b. Multiple Discriminant Analysis

Discriminant analysis is a multivariate technique that may be used to predict group membership [Kachigan, 1982]. The technique is similar to a multivariable regression analysis. Unlike multivariable regression, however, discriminant analysis computes a criterion variable which is qualitative vice quantitative. For example, in a multivariable regression analysis we may try to predict the hardness of ice based on a number of observed descriptors: V_1= ice temperature, V_2= ice salinity, V_3= ice age, etc. These variables may be combined in some manner to arrive at an ice hardness score. The regression equation would look like: $H(t,s,T,...) = \beta_1 V_1 + \beta_2 V_2 + \beta_3 V_3 + ...$etc., where β_n is a weight applied to the variables. In regression analysis the goal is to predict some $H(t,s,T,...)$ for given values of V_n. In discriminant analysis the goal is to classify or group objects based on the same set of observed variables. In discriminant analysis instead of using the regression to arrive at a quantitative "criterion variable", a "qualitative" dummy variable is used to assign group membership. Returning to the previous example using ice hardness, the discriminant equation might appear as $L = \beta_1 V_1 + \beta_2 V_2 + \beta_3 V_3 + ...$etc. where L is a "qualitative" criterion variable and the descriptors are usually considered qualitative in nature. A input data matrix for discriminant analysis of three groups might appear as in Figure 11. An element is assigned to a class based on its value of the "qualitative" dummy variable. For example all elements with criterion variable L between L_1 and L_2 are assigned to one class while all elements with L between L_2 and L_3 are assigned to another class. The class boundaries are chosen by natural groupings in the data.

Groups to be discriminated	Objects within the groups	Scores on the predictor variables			
		x_1	x_2	$\cdots$	x_k
Group A	Object A_1			$\cdots$	
	Object A_2			$\cdots$	
	$\vdots$				
	Object A_m			$\cdots$	
Group B	Object B_1		$\cdots$		
	Object B_2		$\cdots$		
	$\vdots$				
	Object B_n			$\cdots$	
Group C	Object C_1		$\cdots$		
	Object C_2		$\cdots$		
	$\vdots$				
	Object C_l			$\cdots$	

Figure 11. Input data matrix for a discriminant analysis [from Kachigan, 1982].

(1) Limitations on Discriminant Analysis

The validity of a discriminant analysis depends on three factors. 1) Selection of strong predictor variables. These variables should have clearly different mean values for the groups to be discriminated. 2) The variance of a given predictor variable is the same in the respective populations from which the groups of objects have been drawn. 3) The correlation between any two predictor variables is the same in the respective populations from which the alternative criterion groups have been sampled

40

[Kachigan, 1982]. For exan.ple, for populations A and B the correlation of descriptor variables V_{A1} to V_{A2} will be the same as the correlation of V_{B1} to V_{B2}.

There are other considerations that will influence the strength of the discrimination. Some of these considerations are sample size, normality, number of outliers, homogeneity, linearity and collinearity. Discriminant analysis assumes that the discriminating variables are normally distributed and that all the linear combinations of these variables are normally distributed [Tabachnick and Sidell, 1989, p. 511]. There are no good ways to check for multivariate normality so the assumption is made that if the variables are normally distributed then the multivariable distribution of those variables will also be normally distributed. Outliers are a problem in discriminant analysis because of their effect on the variance of the variables. One must keep in mind that discriminant analysis is similar to an analysis of variance problem. The researcher must decide if the outliers are true representations of the population or errors in data collection procedures. If some error in the data set is detected and explainable, then omitting the outliers from the discrimination is justifiable. Homogeneity of the variance-covariance matrices can be examined using Box's *M* test [Tabachnick and Sidell, 1989, p. 379]. The procedures for conducting this test are found in most multivariate statistics books. Linearity is assumed and difficult to check for in discriminant analysis. If linearity is not satisfied, there is no significant change in the probability of misclassifying a sample [Tabachnick and Sidell, 1989, p. 379]. Collinearity may occur making matrix inversion unreliable. Collinearity arises when variables $V_1,...,V_n$, are highly correlated with each other and

groups are not as clearly defined as in Figure 10. Collinearity will reduce the strength of a discriminant analysis.

With the aforementioned conditions considered, discriminant analysis will classify each of the observed cases into groups. No provisions are made in this type of classification for dual group membership. Readers concerned with this factor should pursue Fuzzy clustering techniques [Bezdek, 1981]. Most discriminant analysis programs perform the analysis and then compare the discriminated classification with the known classification and provide a classification accuracy and the relative importance that each variable played in the discrimination. These are the two primary pieces of information used in this thesis to determine the optimal descriptors for this data set. Research has recently been conducted by Shokr [1989] using discriminant analysis to examine important statistics in ice classification using SAR data.

Thirteen descriptor variables, Equations (3)-(15), have been selected to characterize the ice for this research. Discriminant analysis will be used to find the best classifiers of the data. These thirteen descriptors must be further reduced to a set that best accounts for the accurate classification of the ice. Exactly what is "best" for ice classification must be quantified. For example, for navigational purposes the designer of a classification algorithm is probably willing to accept a significant probability of falsely classifying the ice as multiyear. In this work "best" is defined as the top three statistically significant descriptor variables that successfully classify the ice and open water groups. The top three variables are selected because they allow easy visualization of classification

42

strength. The next section will address the method by which this ice classification is accomplished.

III. METHODS

This chapter discusses the collection, processing, description and analysis of the SAR data used in this thesis.

A. DATA COLLECTION

The SAR imagery was collected during the Marginal Ice Zone Experiment (MIZEX) in 1987. This experiment was conducted during March and April in the Fram Strait and Greenland Sea. The experiment was conducted in the marginal ice zone in an area bounded by 75°N to 79°N and 5 °W to 5°E.

The SAR data were collected using an uncalibrated X-band, seven-look, 16 m resolution aircraft mounted SAR known as the STAR-2 [Shuchman et al., 1988]. This data set represents the results of 7 different imaging runs. SAR imagery was used by the science teams in real time and recorded onto high density data tapes for future analysis. It is from these high density data tapes that the images used in this thesis were extracted. The fact that the SAR was not calibrated may have some effect on the stability of the univariate statistics, a factor which will be discussed in a later section. Other system specific characteristics are shown in Table II.

The data set used in this thesis was provided by the Environmental Research Institute of Michigan (ERIM) and consisted of subsets of the digital SAR imagery. These images were extracted from the data collected on missions flown on 5-8 April 1987. The areal coverage of these missions are shown in Figures 12-15. The imagery collected was

44

Table II. SAR Sensor Parameters [from Shuchman et al., 1988].

PROPERTY	IMAGING SYSTEM (STAR-2)
Operating Altitude	29,000 ft
Wave length	X-band
Polarization	HH
Processing	Real time
Recording	8 bit, full bandwidth data recording on parallel HDDR
Swath width	
Narrow (Hi-Res)	17 km
Wide (Lo-Res)	63 km
Pixel size	Along track x crosstrack
Hi-Res	4 m x 4 m
Lo-Res	5.2 m x 16 m
Downlink	4 bits
Azimuth looks	7
Lo-Res	16 m x 16 m
	32 m x 32 m

mosaiced and appears on Figures 16-19. The mosaic images were further divided by ERIM into smaller sub-images compose almost entirely of only one class of ice (first-year, multiyear, odden) or water. These smaller sub-image samples vary in size from 5120 km² to 20 km². The sub-images were manually classified and consisted of 16 first-year ice, 18 multiyear, 11 odden and 12 open water files. These files or sub-images are digital representations of the backscatter intensity of the SAR.
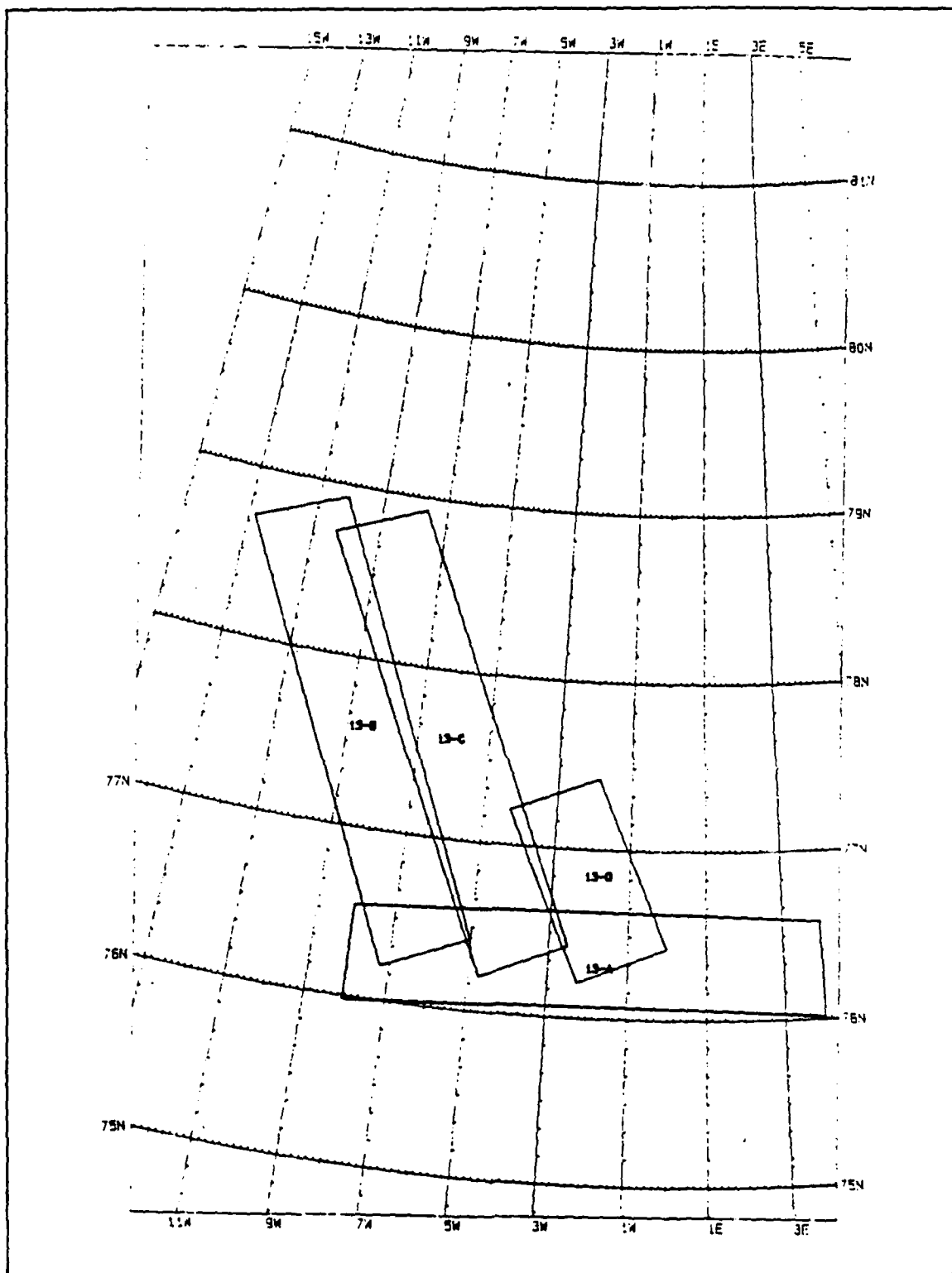
Figure 12. Aerial coverage of mission 13 [from Shuchman et al., 1988].

46
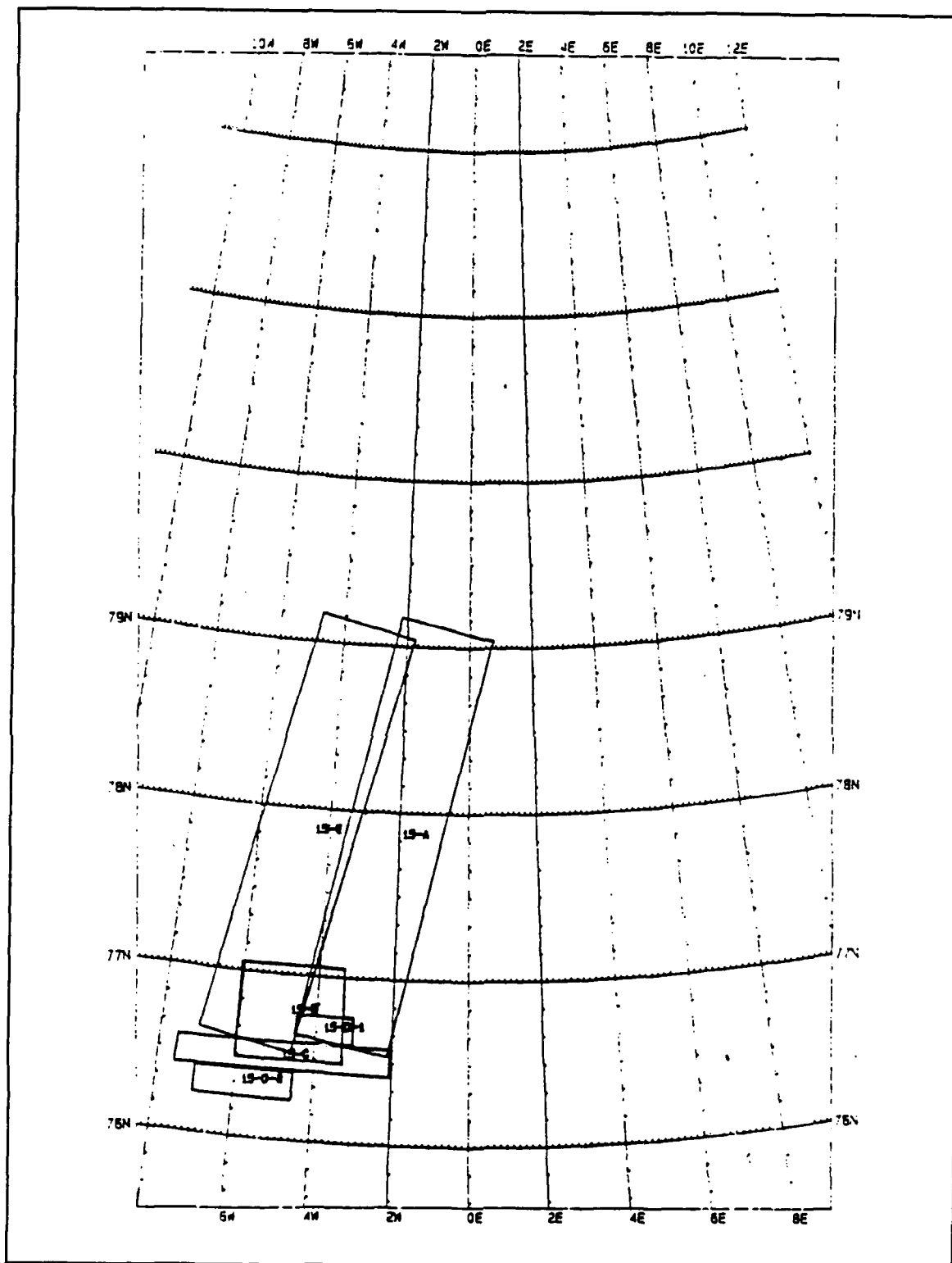
Figure 13. Aerial coverage from mission 15 [from Shuchman et al., 1988]
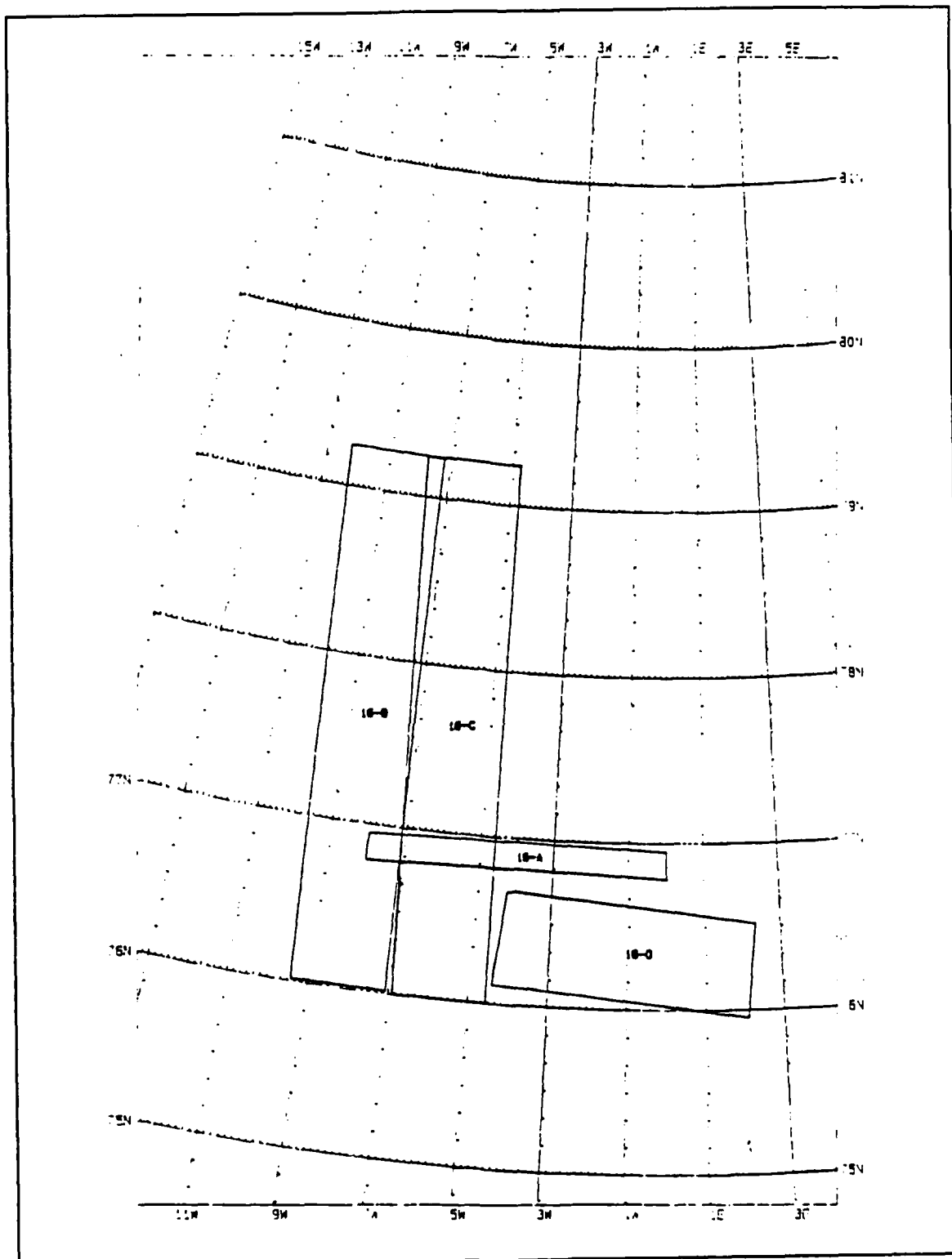
Figure 14. Aerial coverage from mission 16 [from Shuchman et al., 1988].

Figure 15. Aerial coverage of mission 18 [from Shuchman et al., 1988].

Figure 16. SAR image mosaic from mission 13 [from Shuchman et al., 1988].
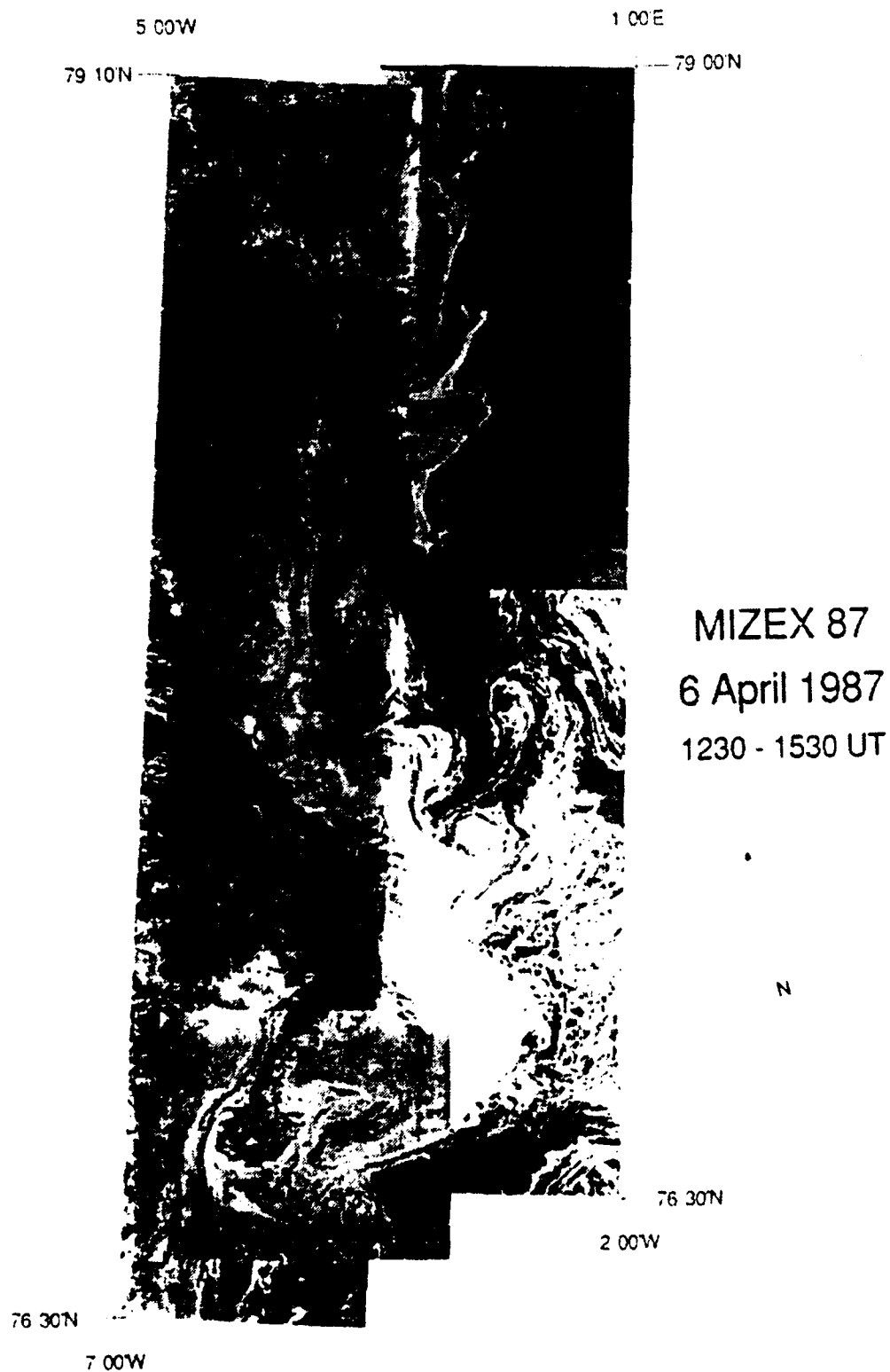
Figure 17. SAR image mosaic from mission 15 [from Shuchman et al., 1988].

MIZEX 87

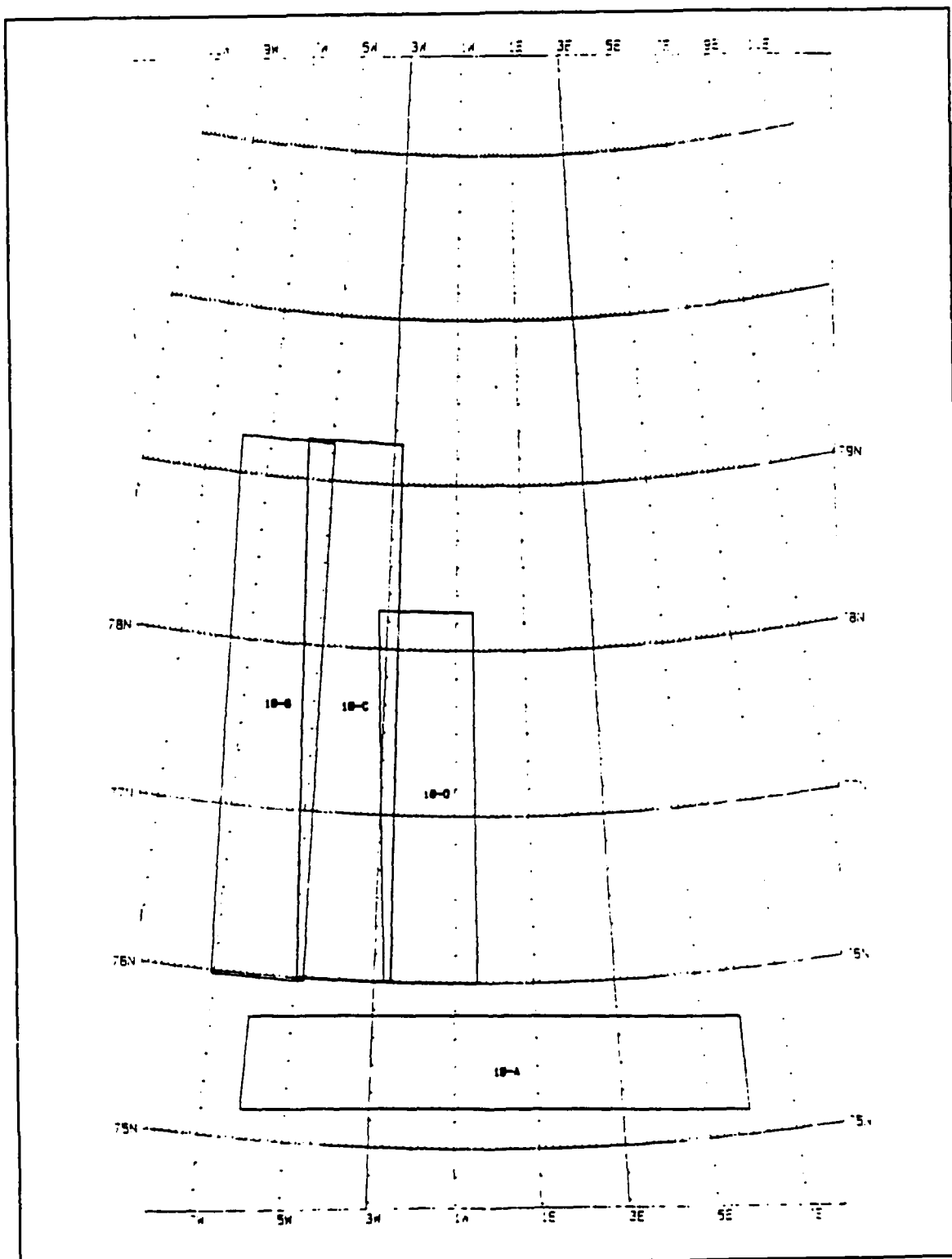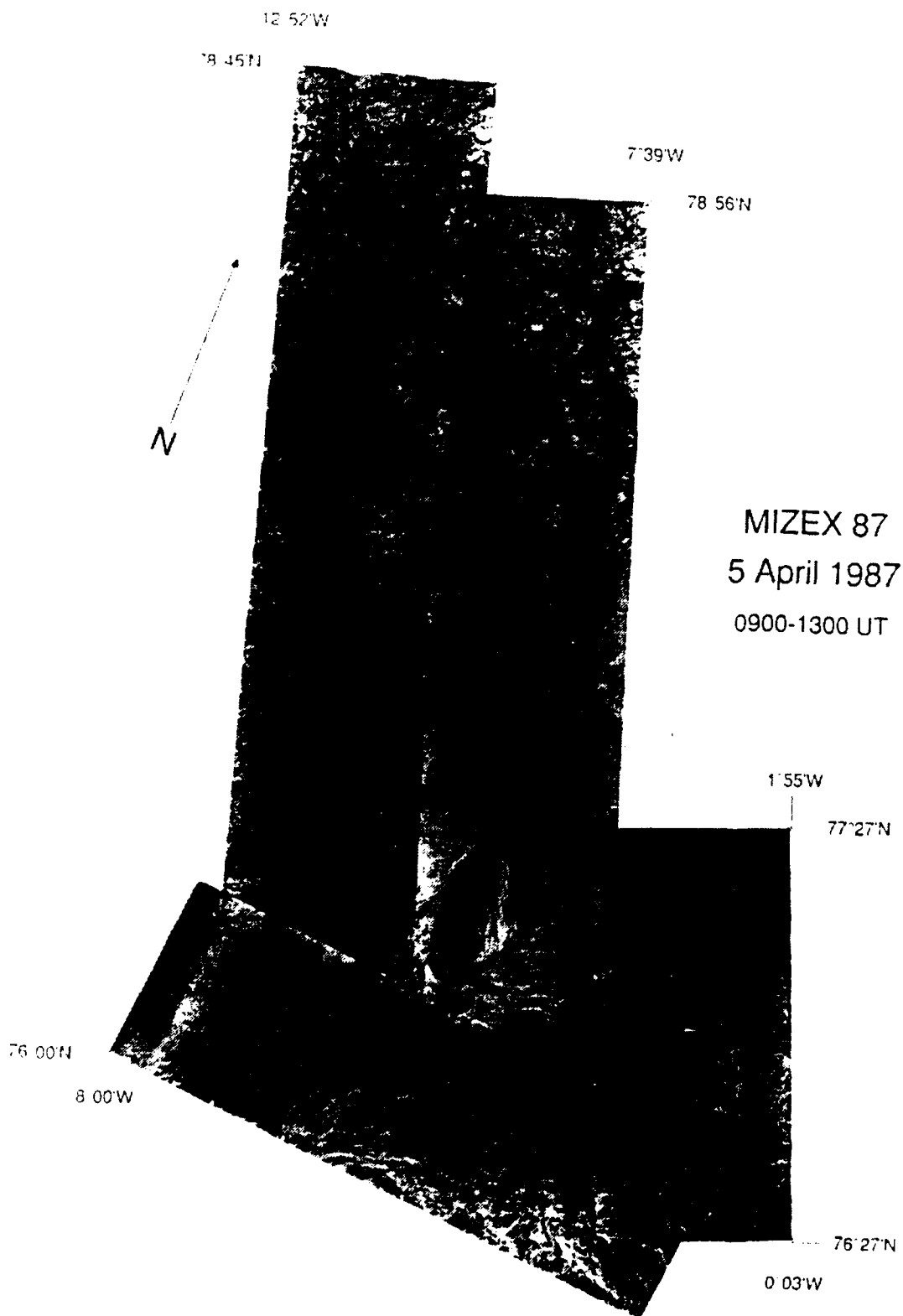**7 April 1987**

1100-2030 UT

Figure 18. SAR image mosaic from mission 16 [from Shuchman et al., 1988].
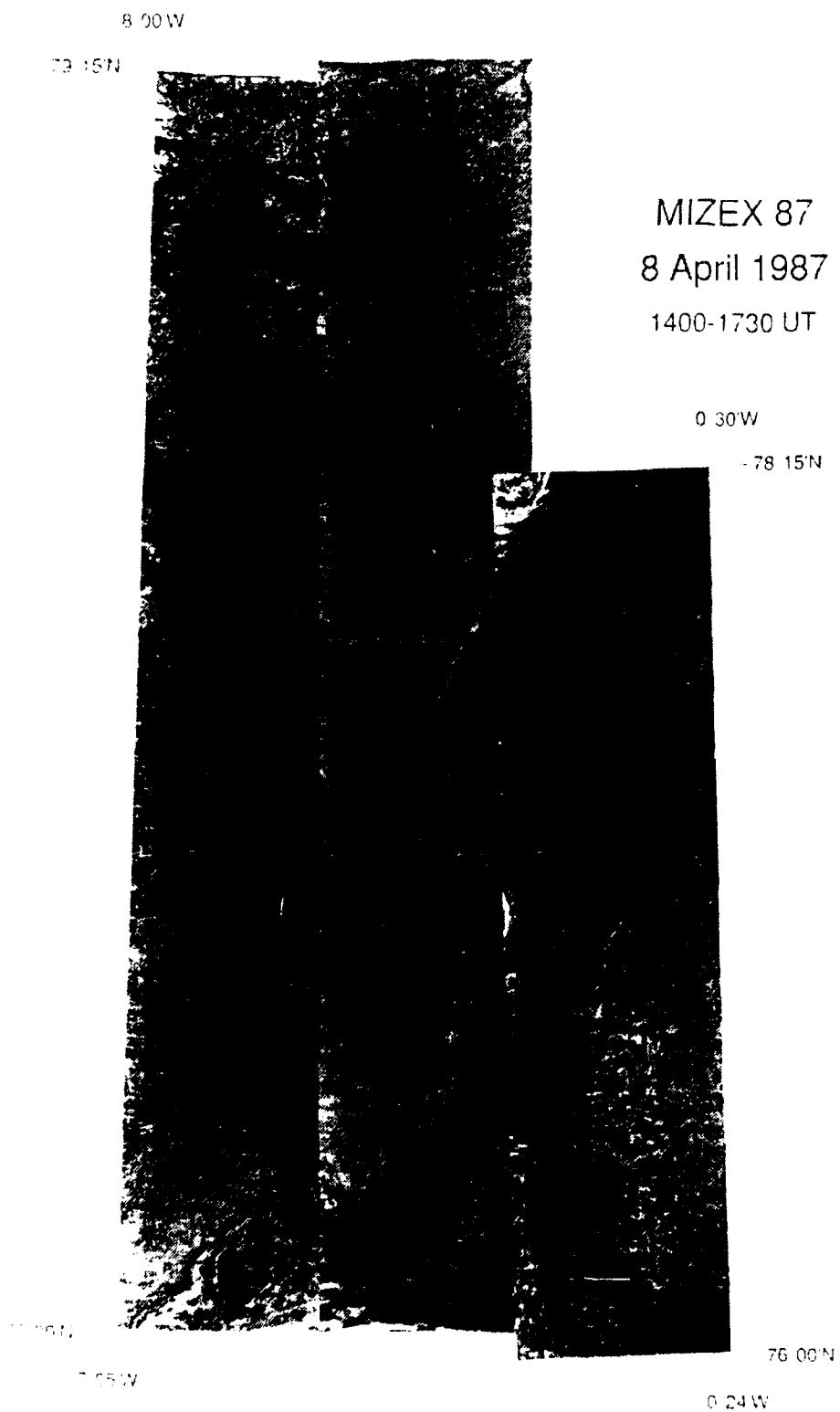
Figure 19. SAR image mosaic from mission 18 [from Shuchman et al., 1988].

B. HARDWARE AND SOFTWARE

The digital sub-images were installed on two computer systems for analysis, the Naval Postgraduate School mainframe and an image display system. Most of the analysis was performed on the mainframe making use of IMSL STAT LIBRARY functions where possible. Discriminant analysis and principal component analysis were also performed on the mainframe using a statistical package, SPSS-X. The image display system was used to view files with questionable characteristics as part of the screening phase.

C. DATA ANALYSIS

Analysis of the data was performed in three main steps. Investigation of the univariate characteristics of the data was performed first, followed by creation of GLC matrices and lastly analysis of the statistical properties of the data using discriminant analysis.

1. Data Screening

The fundamental properties of the data set were examined by producing the univariate characteristics (mean, standard deviation, skewness, kurtosis, etc.) of the raw images. The univariate statistics provided a sense of the distributional characteristics of the sub-images. The univariate statistics and data file sizes were checked against information provided on the data set by ERIM to ensure that they were properly installed.

The focus of this investigation was to find the optimal statistical descriptor or descriptors for the three different ice types and open water. The creation of GLC

matrices was an integral part of this analysis. The three questions addressed prior to creating the GLC matrices were:

- How large an area is needed to capture the texture of the ice? (The image area was selected by ERIM when they manually classified sub-images. These data images are the initial data for this thesis.)

- What vector direction (θ) should be used to generate the GLC?

- What vector length (d) should be used to generate the GLC?

The second two questions are addressed in the following sections.

2.   Vector Direction Investigation

The vector direction employed to create GLC matrices was investigated to ensure that the statistics generated from the GLC would be rotationally invariant. This investigation of directionality is important because ice in the MIZ may be imaged in any number of orientations resulting in a lack of consistent directional features. For example, odden ice demonstrated clear directional features with a 16 pixel periodicity, or 96 m in ground resolution, but the orientation of these features in each image was variable. These linear features are visible in the odden ice as streams of pancake ice aligned by wind or wave forcing. By removing the directional sensitivity of the GLC matrix, any variance due to the orientation of textural features will be removed.

Sample image files from each ice type were examined for directional dependence of the texture measures. This analysis was performed by creating GLC matrices with a vector $\Phi_1(d,\theta)$, where d was fixed at 10 pixels and the angle θ was varied from 0°-180°. The length of 10 pixels was randomly chosen. GLC matrices were

55

computed for each GLC as θ was swept through the 180° arc. The texture statistics were then plotted against θ to search for directional sensitivity.

Figures 20-23 display two important pieces of information, the directionality of the texture statistics and the effect of increasing the number of vectors used in making GLC matrices. Note the reduction in variance as the number of vectors increases from one vector to two vectors ($\Phi_1(d,\theta)$, $\Phi_2(d,\theta)$) separated by 126°, three vectors ($\Phi_1(d,\theta)$, $\Phi_2(d,\theta)$, $\Phi_3(d,\theta)$), separated by approximately 66° and four vectors ($\Phi_1(d,\theta)$, $\Phi_2(d,\theta)$, $\Phi_3(d,\theta)$ $\Phi_4(d,\theta)$), separated by approximately 37°. GLC matrices created with one or more vectors perform an averaging function. As the number of vectors used in generating the GLC increases, the directional nature is reduced. The directional nature of GLC matrices generated with one vector is evident in some of the statistics (Figures 20-23). Note that as the number of vectors increases, the variance of the statistic approaches some mean value regardless of the orientation of the sets of vectors.

Selection of the appropriate number of vectors to remove the directional sensitivity was studied next. This was done under the hypothesis that some optimal set of vectors could be identified that removed the directional dependence and kept the computation time to a minimum. Computational costs increases with each vector that is used in creating the GLC matrices. Reviewing Figures 20-23, it appears that most of the directional variance was removed by using two vectors. This is evident because most of the large excursions exhibited by the statistics are removed when the GLC matrices were generated using two vectors.
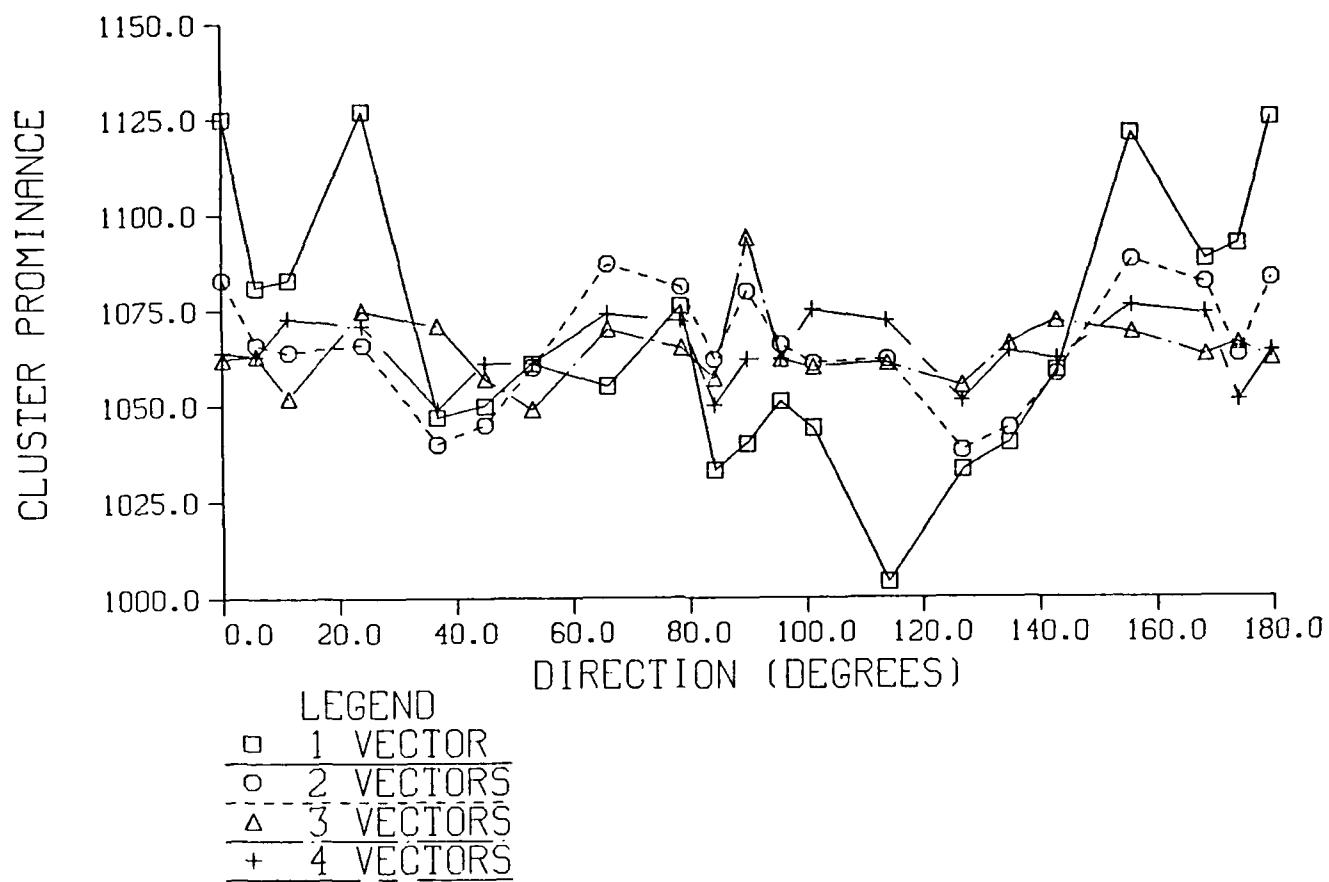
Figure 20. Directionality of cluster prominence for first-year ice.

57
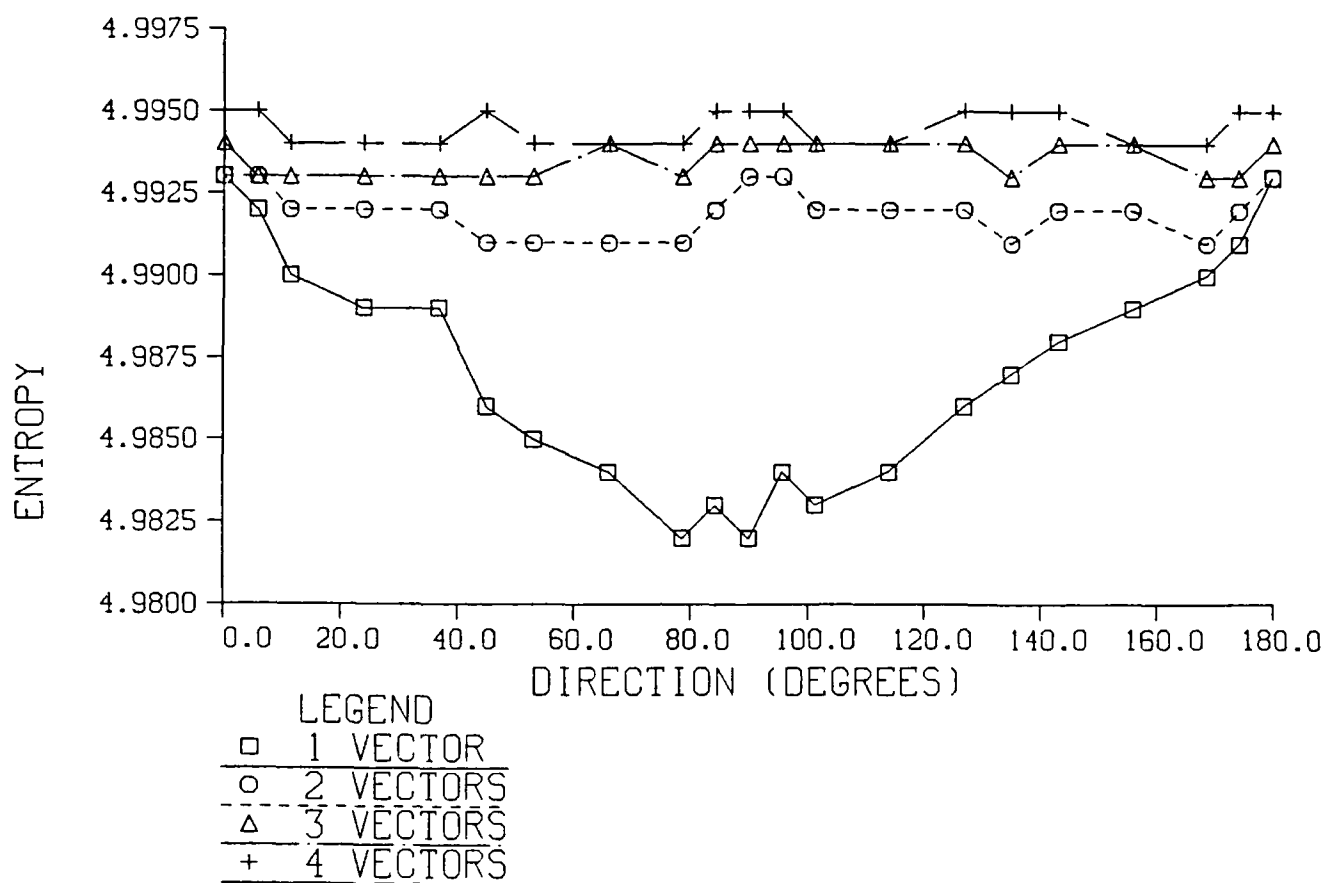
Figure 21. Directionality of entropy for first-year ice. Note the marked directionality of the one vector case.

DIRECTIONALITY OF GLC STATISTICS
ODDEN ICE, FILE 35
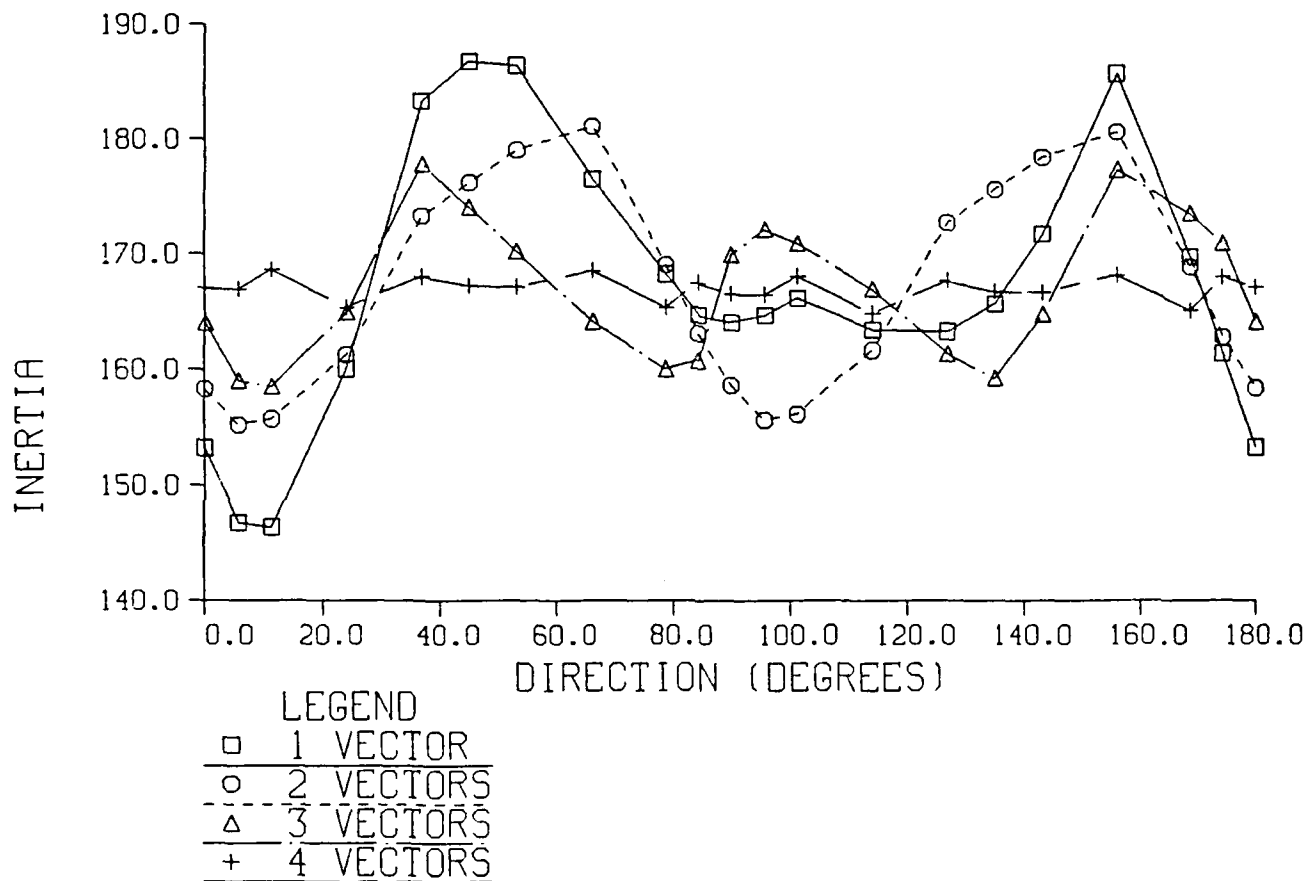
Figure 22. Directionality of inertia for odden ice. Note the reduction in the directional variance as the number of vectors is increased.

59
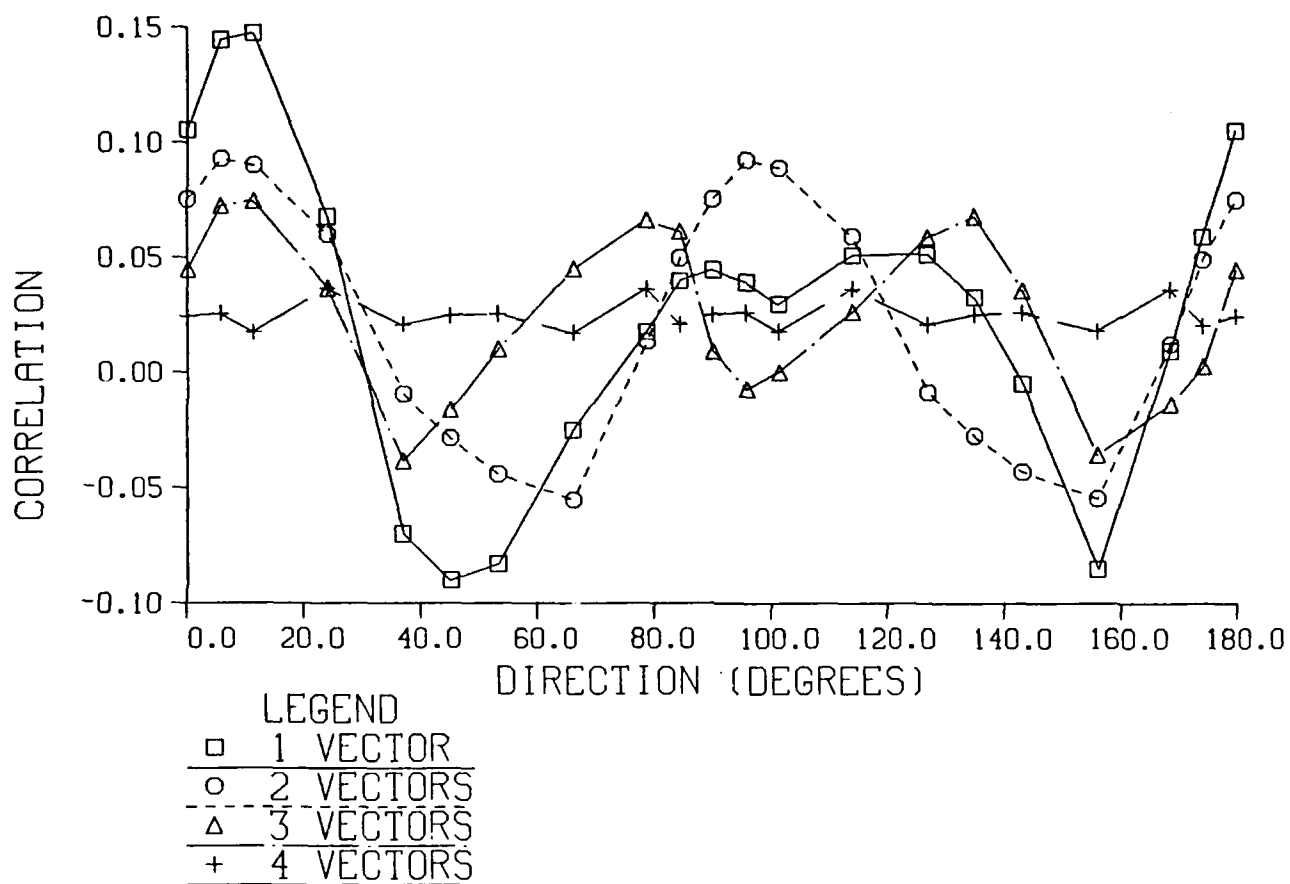
Figure 23. Directionality of correlation for odden ice. Note the reduction in the variance as the number of vectors increases.

This set of plots also indicated which ice types would allow clear separation of the ice types and open water. If these statistics were going to be of use in discriminating between the various ice types and open water, then their statistical measures should be as different as possible. Sufficient separation for open water and first year ice was observed for most texture statistics. However, odden and multi-year ice were difficult to separate. Analysis of the directional variance for these two ice types showed that their values remained within one standard error of each other. By increasing the number of vectors, cluster prominence and inertia became separated by more that one standard error (Figures 24-25). Inspection of these figures determined that three vectors separated by approximately 66° provided a non-directional GLC and subsequently non-directional texture statistics.
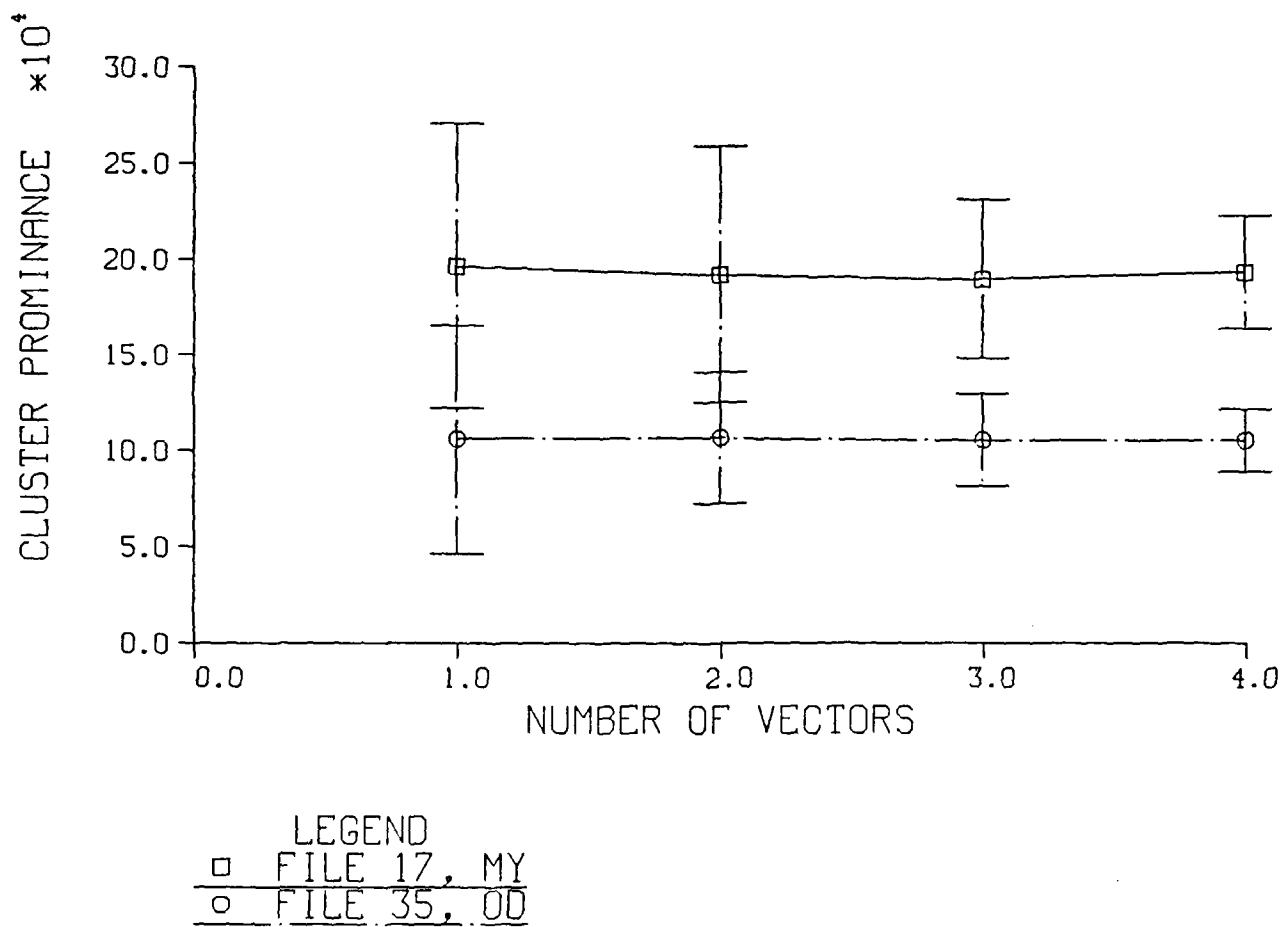
Figure 24. Cluster prominence for multiyear and odden ice. Note the separation greater than one standard error for three vectors.
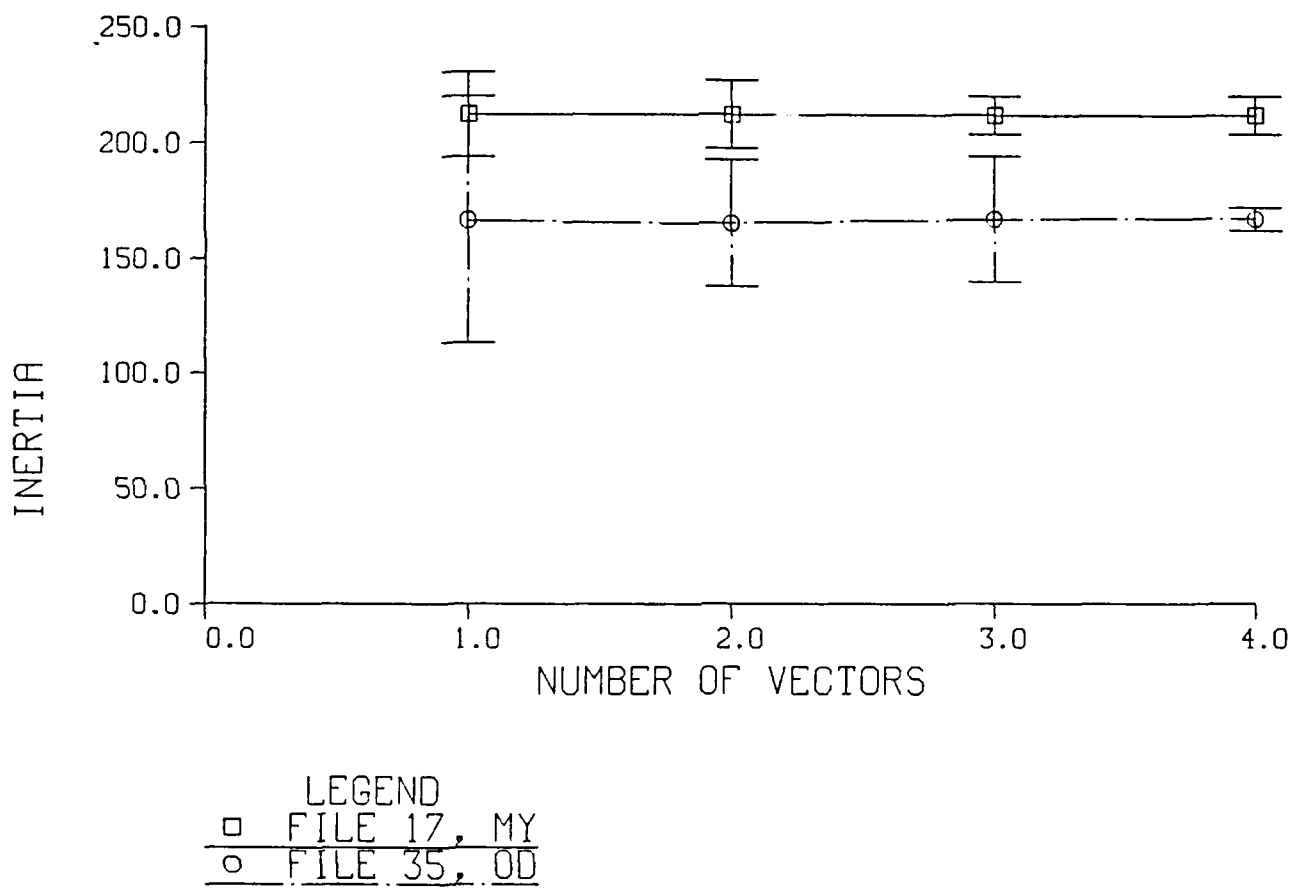
Figure 25. Inertia for multiyear and odden ice. Note the separation of odden from multiyear ice for two or more vectors.

3. Vector Length Investigation

Selection of an optimal vector length was performed by using one vector of increasing length to create GLC matrices and subsequent statistics for sample files from each ice type. The vector length ranged from 1 to 16 pixels which equates to 16 m to 256 m in ground resolution. Most of the texture statistics remained unchanged as the length increased. However, inertia (Figure 26), cluster prominence (Figure 27), local homogeneity (Figure 28) and correlation (Figure 29) showed a marked change with changing length. Each of these statistics depends on the difference in gray shades. Such statistics will be sensitive to changes in the micro-texture. Once the vector is long enough to sample two statistically independent pixels, further lengthening of the vector will no longer change the statistic. Generating GLC matrices that provide a maximum separation of the texture statistics is desired for strong discrimination. Based on these samples, a vector length of four was selected for use in generating the GLC matrices for the study because the texture statistic was most stable for lengths of four or greater.

4. GLC Investigation

GLC matrices were computed for all 57 data files using three vectors of four pixels in length separated by approximately 66°. Representative GLC matrices and the associated raw image for the ice and open water groups may be seen in Figures 30-33. It is clear from these images and their associated GLC matrices that they have unique features. Note that while these images are visually distinct, the challenge is to use their associated GLC matrices to capture the features that allow a human interpreter to discriminate between the different types. Note that the open water and multiyear ice are
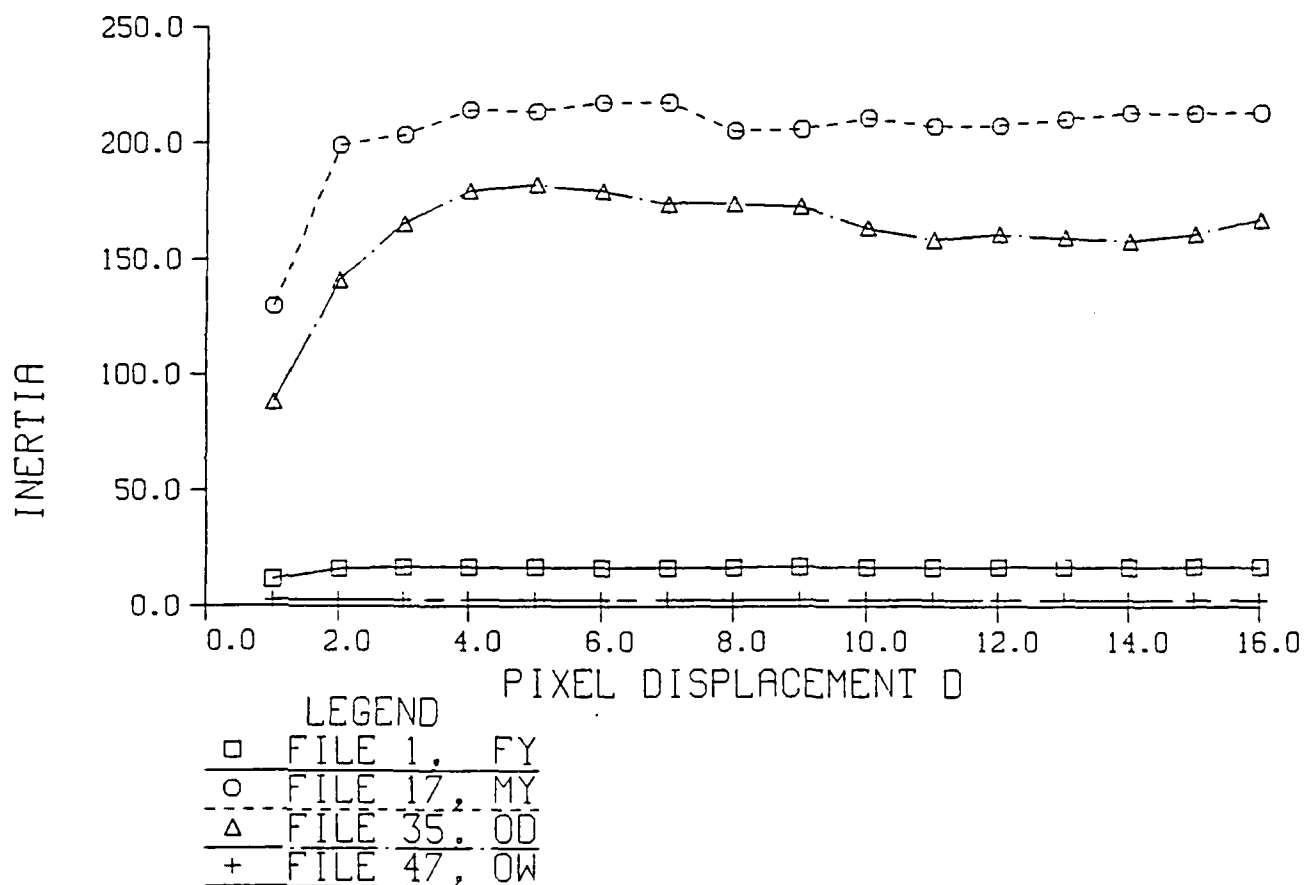
Figure 26. Vector length effect on inertia. Note that inertia appears unaffected by length after a displacement of four pixels. Each pixel represents 16 meters in ground resolution.

65
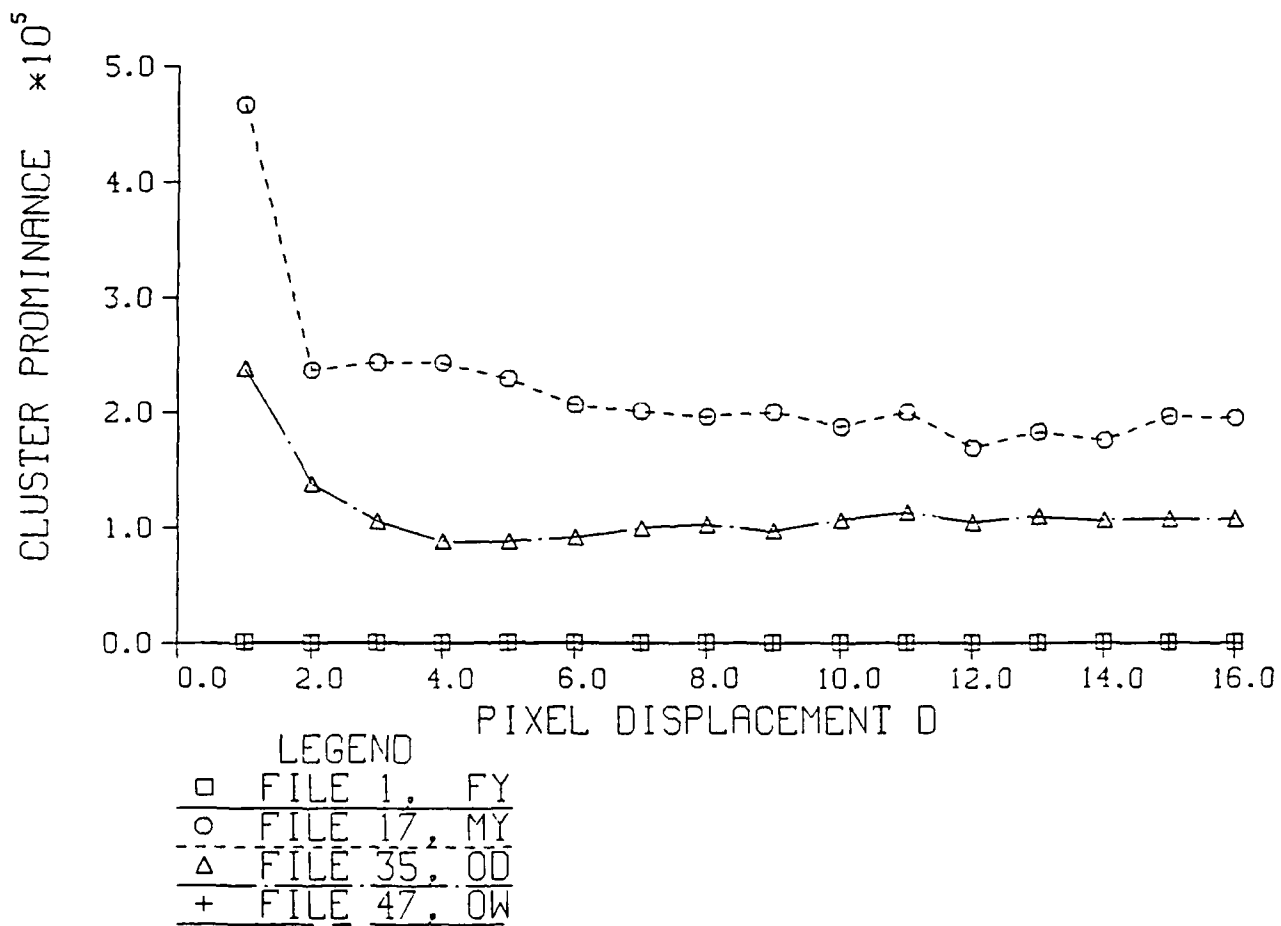
Figure 27. Vector length effect on cluster prominence. Note that cluster prominence appears unaffected by length after four pixels displacement. Each pixel represents 16 meters in ground resolution.

66
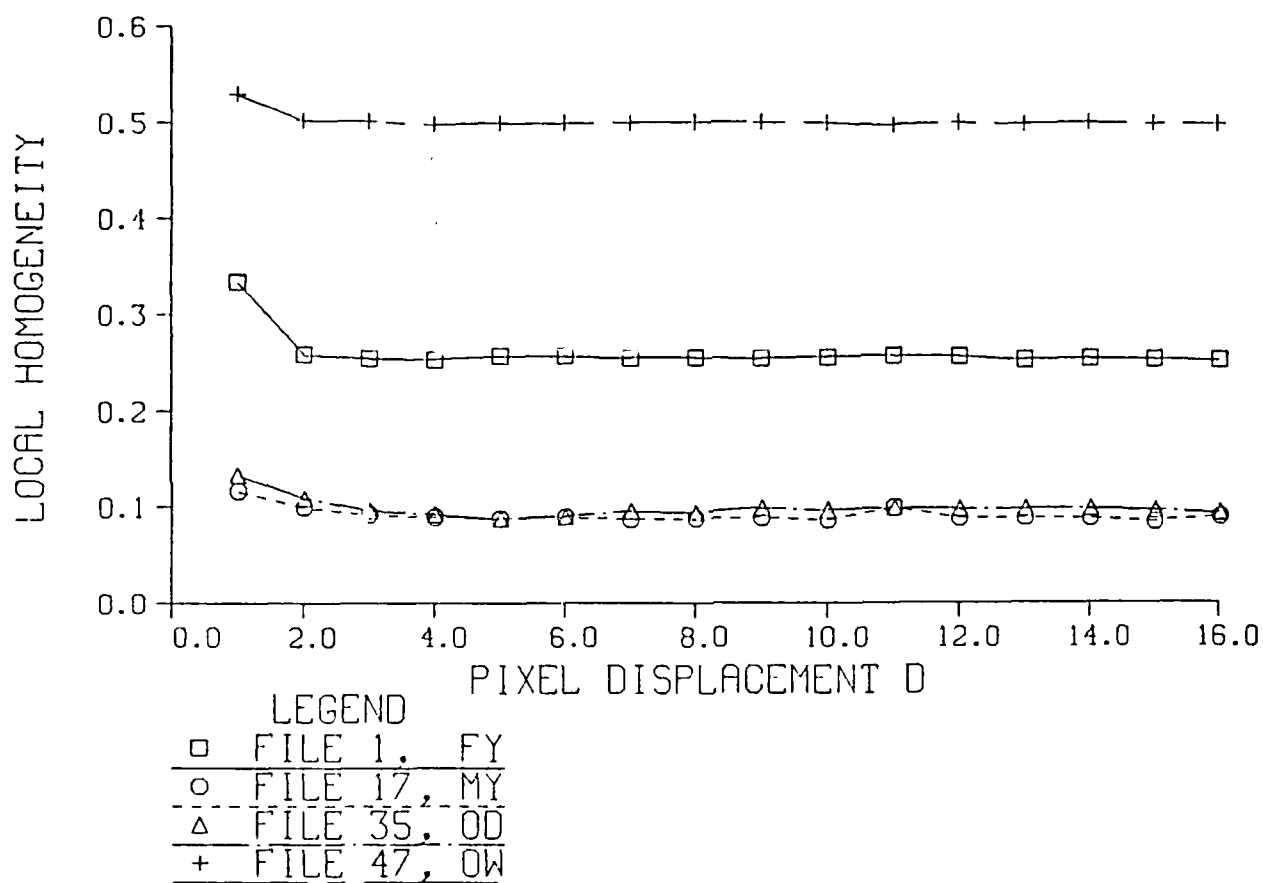
Figure 28. Vector length effect on local homogeneity. Each pixel represents 16 meters in ground resolution.
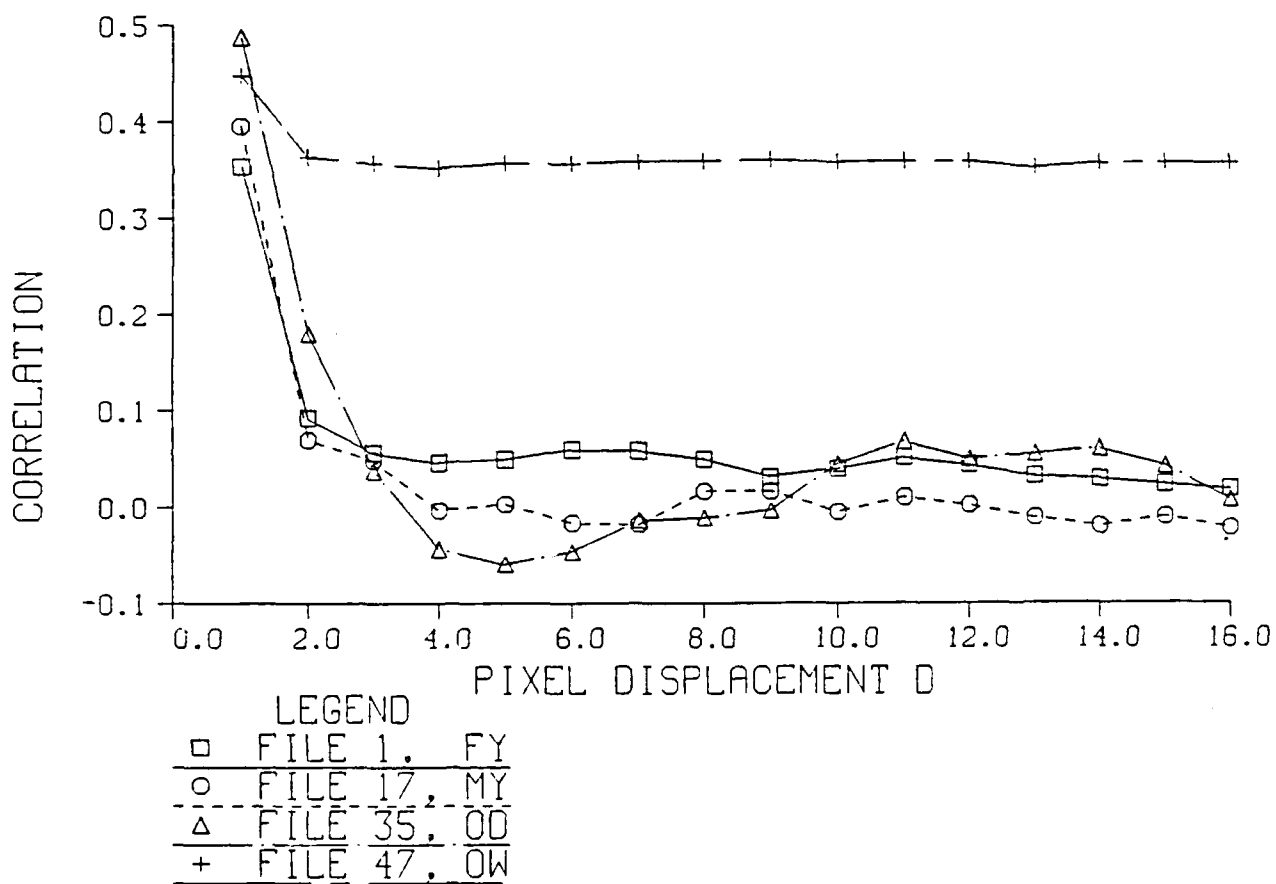
Figure 29. Vector length effect on correlation. Note that open water is relatively unchanged by an increase in displacement. Each pixel represents 16 meters in ground resolution.
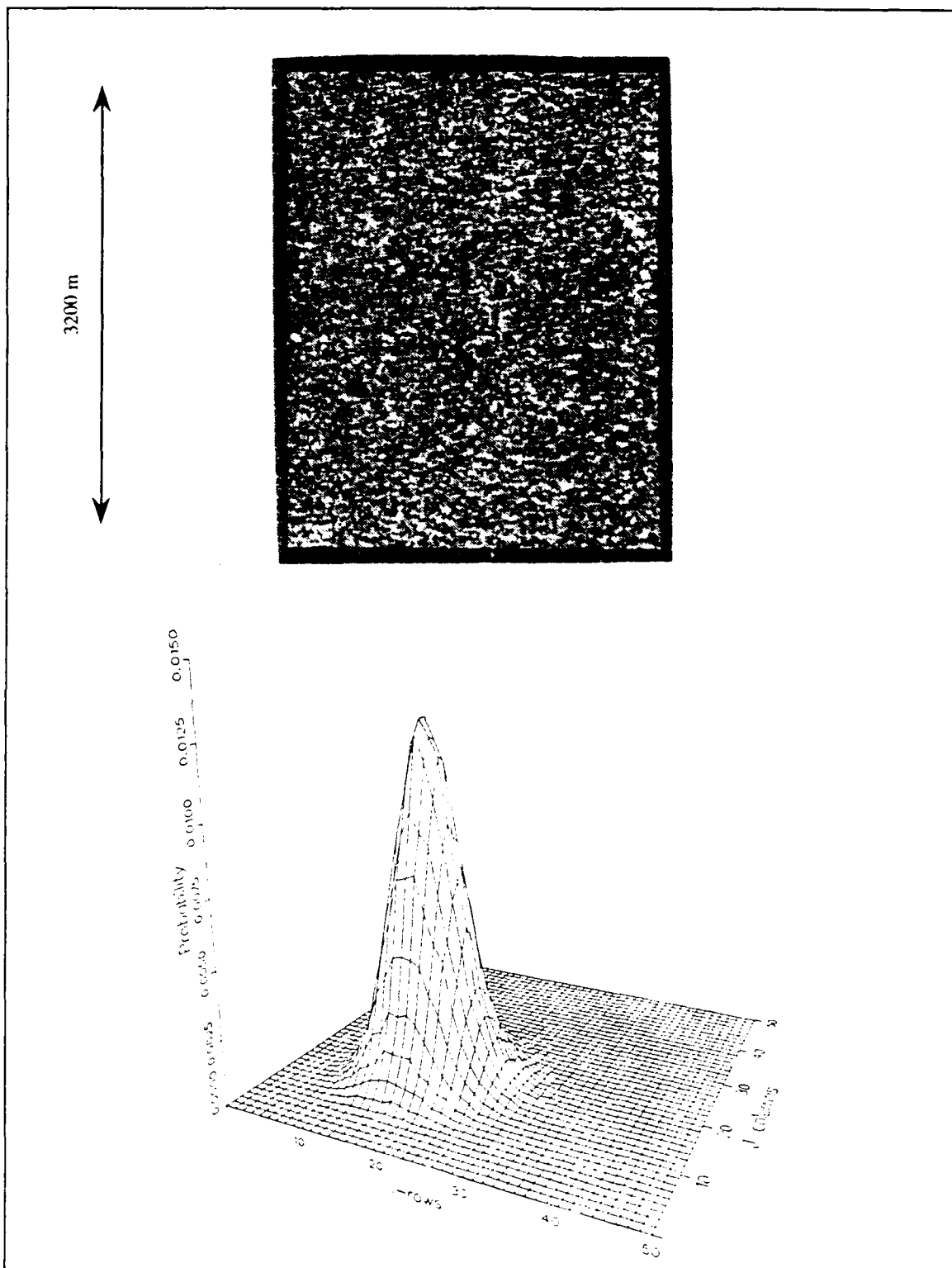
Figure 30. First-year ice image and associated GLC

69
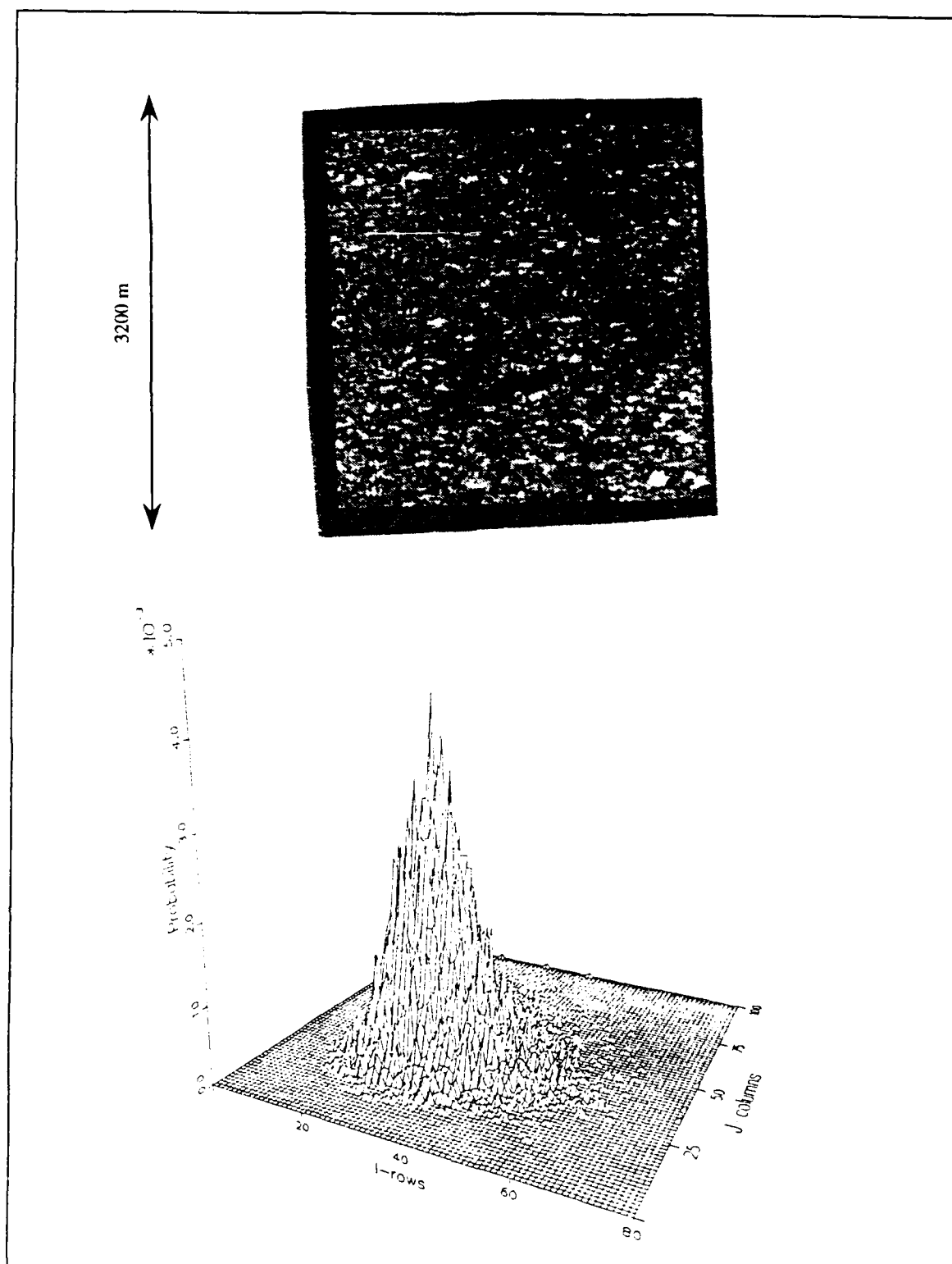
Figure 31. Multiyear ice and associated GLC

3200 m

Probability

*10⁻⁴

25.0

20.0

15.0

10.0

5.0

0.0

J-columns

80

75

50

25

I-rows

10   20   30   40   50   60   70   80
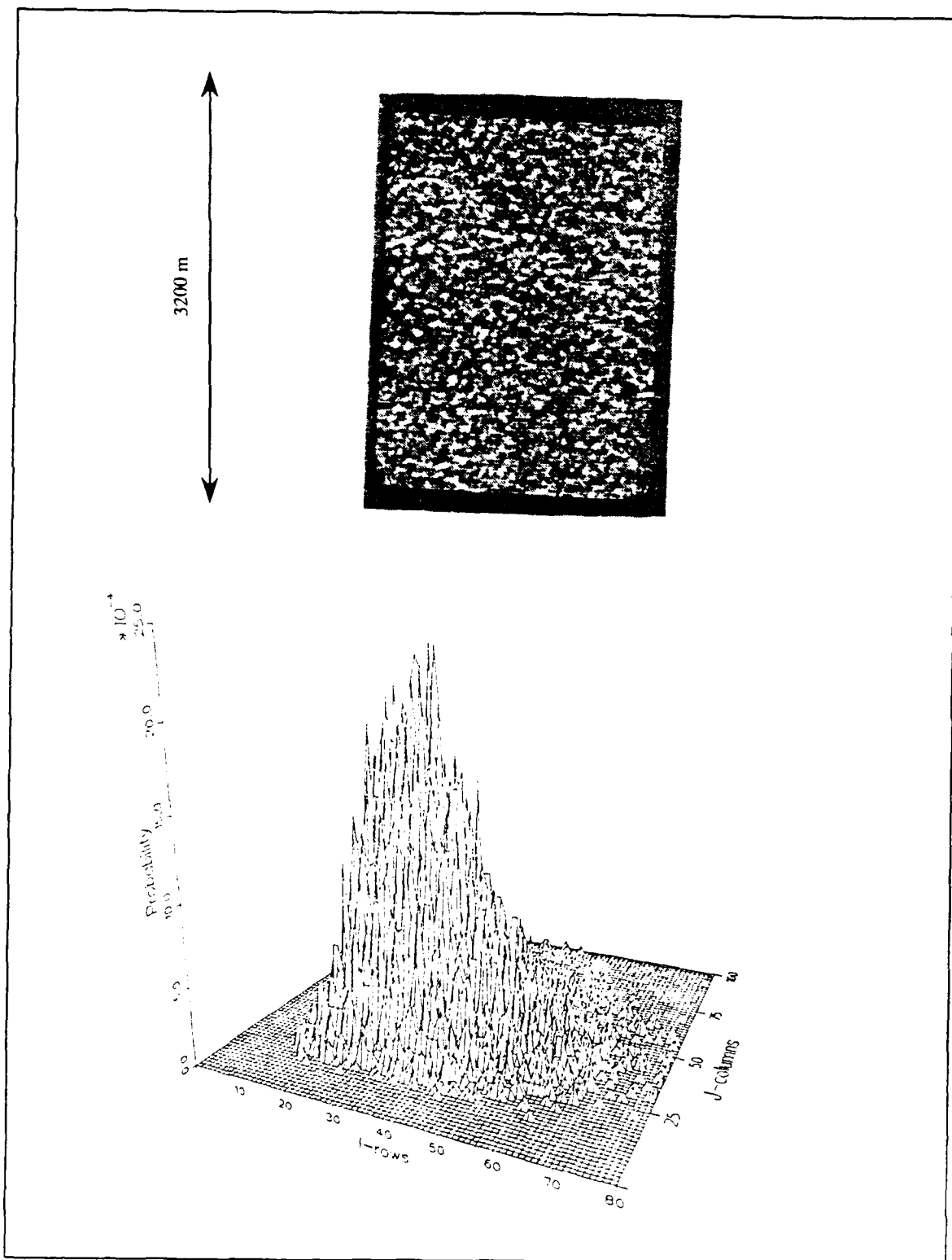
Figure 32. Odden ice and associated GLC.

71
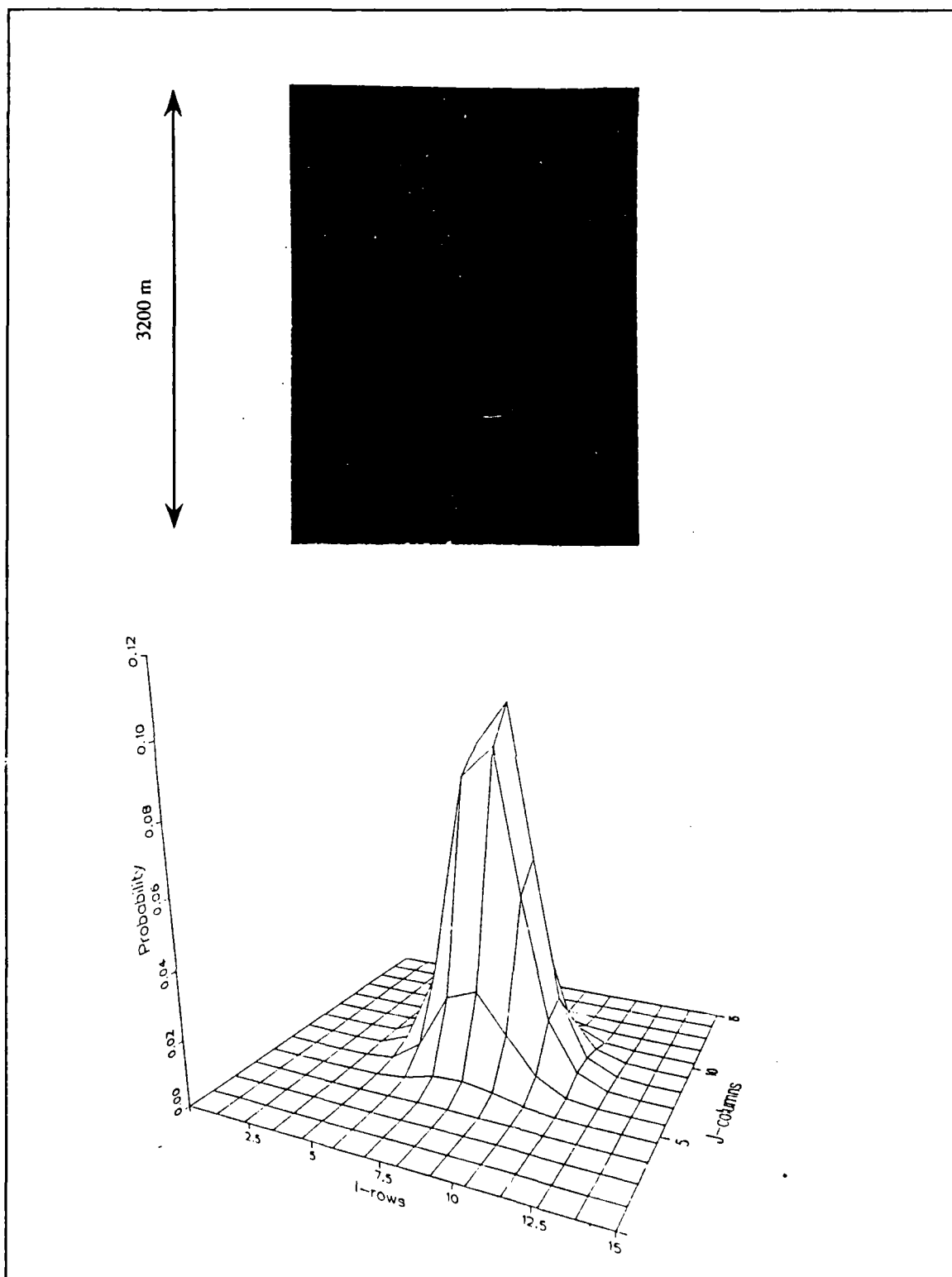
Figure 33. Open water and associated GLC.

72

distinctly different in brightness. These two represent opposite ends of the spectrum in terms of brightness values and most of the texture statistics. However, differentiating between multiyear ice and odden is challenging. Human interpreters are able to identify odden without much difficulty due to the linear features in the image.

The statistics generated from the GLC were combined into a data file that was to be used in discriminant analysis. Before using this data file it was checked to see if it met the requirements for a strong discriminant analysis (see section: Limitations on Discriminant Analysis). Recall that among other things, the variables should be normally distributed. The distributions of the statistics were examined. Most of the distributions for the statistics appeared normal but some clear outliers were found.

In an effort to improve the distribution of the statistics each image was divided in half, doubling the sample size. It was possible to increase the sample size because the original ice sub-image sizes were randomly chosen and independent. The outliers were removed and the distribution was rechecked. This now formed a smoothed data set that would permit optimum discrimination. This step was necessary in order to be sure that the discriminant analysis identified as clearly as possible two things: the group centroids for each ice type and open water and the optimal descriptor variables responsible for the locations of the centroids. The smoothed data set consisted of 28 first-year, 34 multi-year, 18 odden and 22 open water files. Other requirements for strong discriminant analysis were satisfied. The optimal statistics identified by discriminant analysis with this smoothed data set were then applied to the unsmoothed data to assess classification accuracy. The unsmoothed data set will be referred to as the original data set.

5. Discriminant Analysis

Discriminant analysis was performed on the smoothed data set to identify the optimal discrimination statistics. These optimal statistics were then used on the original data set to assess classification accuracy of the discrimination.

To identify the optimal statistics stepwise discriminant analysis was used. A stepwise discriminant analysis tests each variable one at a time to see how much it improves the separation of the group centroids. The variables that most clearly separate the groups are brought into the analysis first. The process continues until the improvement in discrimination is not considered significant. In this study the descriptor variables were brought into the analysis if they were significant at the $p=0.01$ level. The relative importance of each discriminating variable is provided by Mahalanobis distance D^2. The term D^2 can be interpreted as the squared distance between the means of a variable [Afifi and Clark, 1984]. This provides a measure of how far each variable will separate the different ice classes. The larger the D^2 the better the statistic separates the groups.

Classification accuracy is computed when the stepwise analysis ends and the observations have been placed into groups. The accuracy is determined by comparing the actual group membership with that provided by the discrimination.

IV. DISCUSSION

After applying the optimal GLC vector described in Chapter III, texture statistics for each image were then calculated. Within each ice class the mean and standard deviation for each statistic were also calculated. The results are shown in Table I. A chosen statistic will be able to discriminate between ice types if the mean values for the statistic are clearly separated. For example, with the mean intensity (an univariate statistic), the mean value for first-year ice is 16.8 ± 6.5. This centroid is clearly different from multiyear ice, 33.7 ± 6.2, and open water, 8.0 ± 0.2. Unfortunately, odden ice, 31.3, can not be clearly separated from multiyear ice, so the mean intensity cannot be used by itself to classify these four ice types. In fact, a review of Table III shows that no single variable is sufficient by itself; range appears the most promising.

Many combinations of the univariate statistics exist that can be used to classify the various ice types and open water. For example, the centroid located by the mean intensity and the univariate statistic, standard deviation, shows, some classification skill (Figure 34). As the number of statistics used in classifying the groups of ice and water increases, the possible number of combinations increases geometrically. Stepwise discriminant analysis of the smoothed data set quantifies which statistics are most important in classifying the ice. If the smoothed data set is used, this data set should define the "true" mean for each statistic more accurately than if the original data set were used. Table IV shows the results of the discrimination on the smoothed data set. The

75

Table III. Texture and Univariate Statistics. Mean Value and Standard Error for the Original Data Set.

	ICE TYPE			
	FIRST-YEAR	MULTIYEAR	ODDEN	OPEN WATER
MEAN	16.79 ± 6.48	33.70 ± 6.16	31.28 ± 3.13	8.04 ± 0.18
VAR	1.52 ± 42.67	109.12 ± 71.72	81.41 ± 26.49	1.68 ± 0.39
STDV	4.78 ± 3.00	10.11 ± 2.68	8.92 ± 1.39	1.29 ± 0.14
SKEW	0.49 ± 0.35	1.06 ± 0.43	0.69 ± 0.14	0.47 ± 0.92
KURT	0.74 ± 0.95	3.00 ± 2.39	0.82 ± 0.34	3.10 ± 11.73
RANGE	41.28 ± 34.19	98.86 ± 25.69	70.32 ± 12.63	10.42 ± 4.04
CFVAR	0.27 ± 0.07	0.30 ± 0.05	0.29 ± 0.04	0.16 ± 0.01
INERT	54.69 ± 68.18	204.32 ± 136.99	158.01 ± 50.28	3.23 ± 0.68
CLPRO ($\times 10^4$)	7.31 ± 17.93	40.10 ± 79.65	11.36 ± 8.54	0.0085 ± 0.0059
LHOMO	0.21 ± 0.07	0.10 ± 0.02	0.10 ± 0.01	0.48 ± 0.03
ENERG ($\times 10^{-3}$)	7.33 ± 5.57	1.23 ± 0.51	1.24 ± 0.29	0.54 ± 0.10
ENTRO	5.57 ± 0.97	7.11 ± 0.38	7.01 ± 0.25	3.26 ± 0.19
CORLA	0.08 ± 0.06	0.07 ± 0.05	0.03 ± 0.04	0.17 ± 0.17

step at which these variables are included in the discrimination is determined by how much strength they add to the separation of the groups of ice and open water. This table shows the statistics that were considered significant for an F-test conducted at the $p=0.01$ level. This restrictive criterion helps remove variables that add little strength to a

STANDARD DEVIATION VS MEAN

1=FY, 2=MY, 3=OD, 4=OW
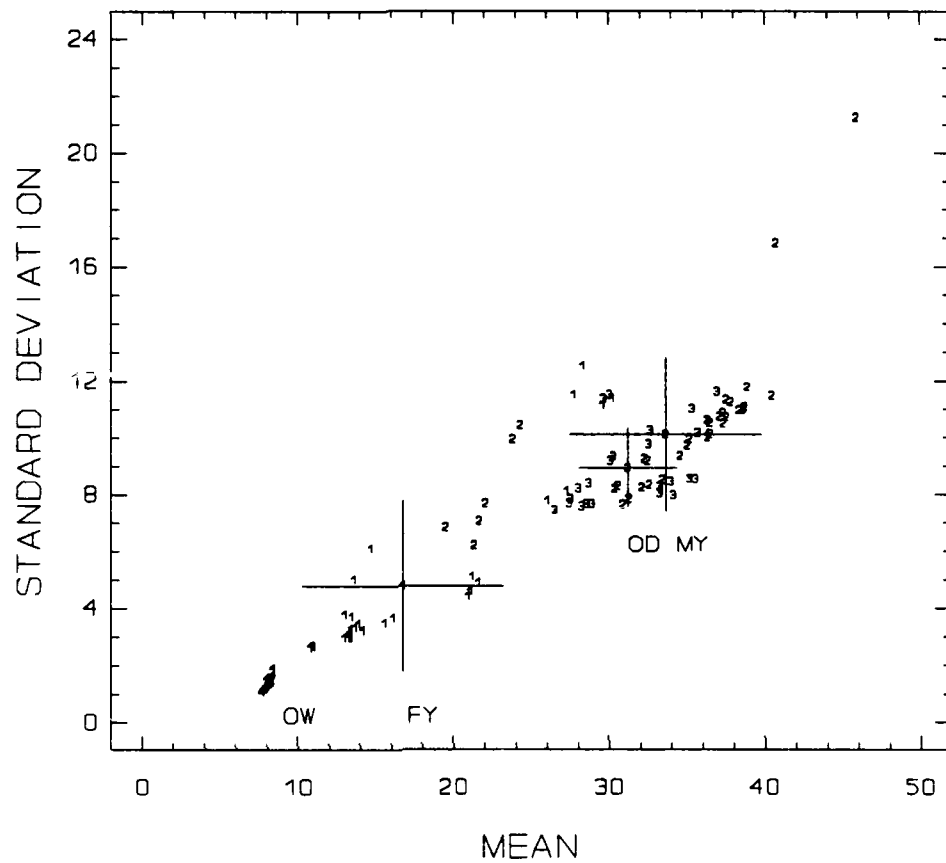
Figure 34. Mean versus standard deviation for original data set. Note the poor separation of the multiyear and odden ice.

discrimination.

Analysis of the smoothed data set with the combination of texture and univariate statistics revealed that range was the strongest discriminating variable. Range classified the smoothed data with better than 86% accuracy for all groups. Additionally, range was the only variable that was considered significant at the p=0.01 level in discriminating multiyear ice from odden ice for the smoothed data set. The next step brought entropy

into the discrimination. Local homogeneity and kurtosis were omitted from an analysis of the smoothed data set with texture and univariate statistics, respectively, as they were not considered statistically significant for inclusion in the discrimination. While local homogeneity was not considered significant when discriminating with the texture statistics alone, it was included in the analysis when both texture and univariate statistics were combined.

The mean classification accuracy is a measure of how well the analysis classified all the ice and open water groups for a given group of statistics and can be used to provide a relative comparison of the strengths of the different groups of statistics. The mean accuracy is the number of cases correctly grouped divided by the total number of cases. The mean accuracy of the classification for the smoothed data is expected to be high because outliers have been removed.

The mean classification accuracies presented in Table IV show that a classification using texture and univariate statistics combined is stronger than a discrimination performed with univariate statistics alone. Additionally, using univariate statistics alone permits classification of the ice types with a significantly higher mean accuracy than the texture statistics alone. It is important to remember that Table IV reflects the relative strength of the variables and their ability to discriminate between the ice types.

The optimal discriminating variables are considered to be the first three variables selected in a stepwise discriminant analysis (Table IV). Plots of the top three variables selected by the stepwise discriminant analysis for each group of statistics are shown in Figures 34-37.

Table IV. Discriminant Analysis Results for Smoothed Data.

	TEXTURE STATISTICS (ALONE)	UNIVARIATE STATISTICS (ALONE)	TEXTURE AND UNIVARIATE STATISTICS (TOGETHER)	MULTIYEAR VERSUS ODDEN[*]
STEP 1	INERTIA	RANGE	RANGE	RANGE
STEP 2	ENTROPY	COEF.OF VARIANCE	ENTROPY	[b]
STEP 3	CLUSTER PROM.	SKEWNESS	LOCAL HOMO.	[b]
STEP 4	ENERGY	MEAN	MEAN	[b]
STEP 5	CORRELAT.	VARIANCE	SKEWNESS	[b]
STEP 6	[b]	STANDARD DEVIATION	CLUSTER PROM.	[b]
STEP 7	[b]	[b]	CORRELAT.	[b]
ACCURACY	86.3%	93.1%	93.1%	86.5%

[*] The discrimination of multiyear ice and odden was performed with both texture and univariate statistics.
[b] A missing entry indicates that no other descriptor variables were significant in a stepwise regression using p=0.01 for the maximum significance of F to enter.

These plots show good separation of the ice types and open water. The center of the cross lines represents the mean value for the particular set of statistics for each ice type or open water; its length represents one standard deviation. Note that the combination of the texture and univariate statistics clearly separates the group centroids for the ice types and open water.

INERTIA VS ENTROPY VS CLUSTER PROMINENCE
Smooth Data

INERTIA
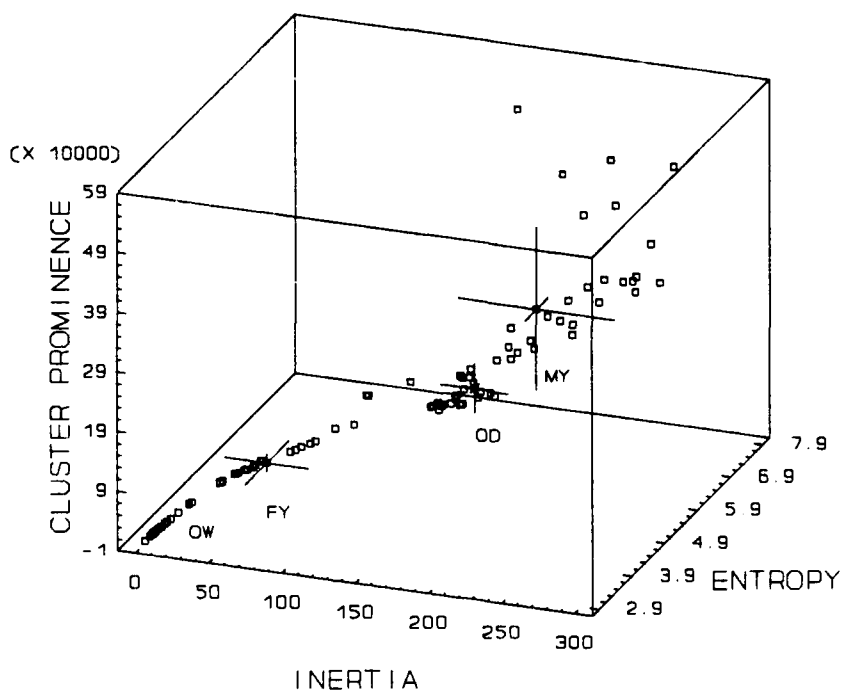
Figure 35. Top three discriminating texture variables for the smoothed data set considering all ice types and open water samples.

The top three statistics in each group of the statistics identified with the smoothed data set were used on the original data set to test their ability to successfully discriminate between the ice types and open water as compared to the use of all the statistics. Table V shows the classification skill for discriminations performed using only the top three statistics from each group. For example, when the texture and univariate statistics are combined, range alone correctly classified 74.6% of the images. When entropy was added, the combination of range and entropy classified 86.0% of the cases correctly. Range alone was able to discriminate the multiyear ice from the odden in 81.0% of the cases.

80
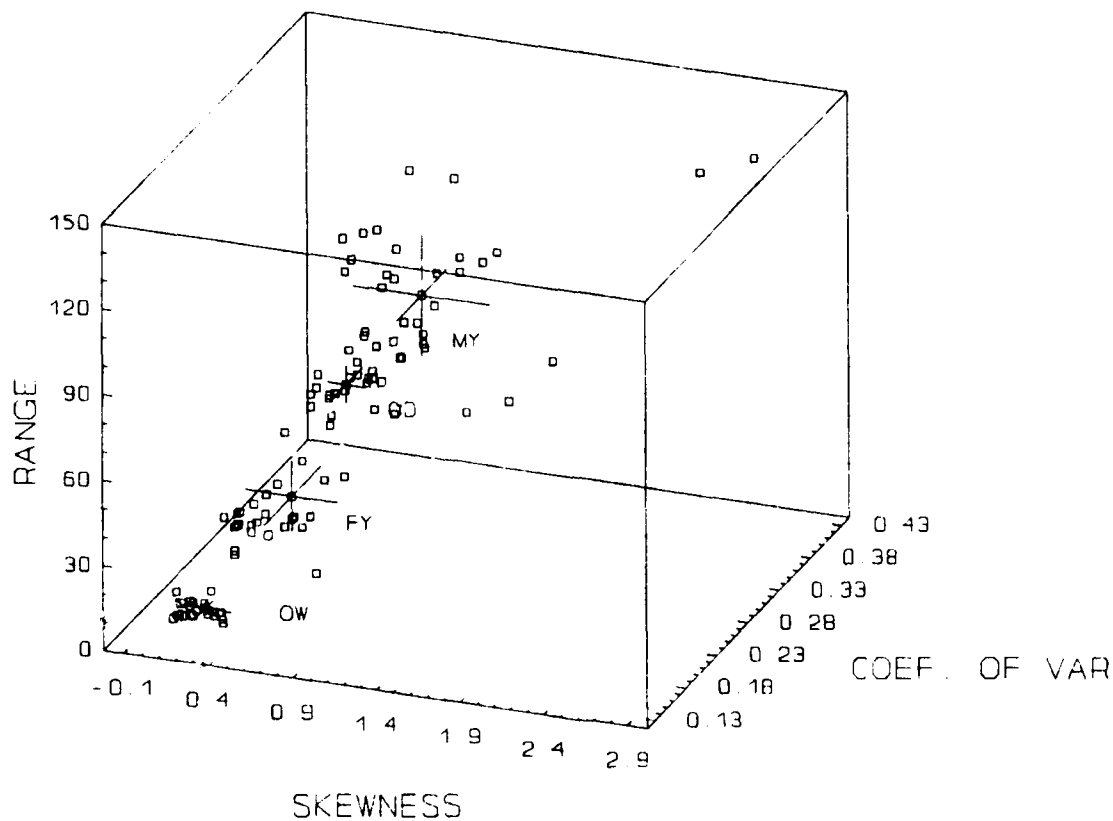
Figure 36. Top three discriminating univariate statistics for the smoothed data set considering all ice types and open water samples.

As was previously mentioned, each statistic that is added in the discrimination improves the separation of the ice type and open water centroids. Plots of inertia vs entropy (Figure 38), range vs coefficient of variance (Figure 39), and range vs entropy (Figure 40) depict the relative strength of each of the top two variables from each of the groups of statistics.

These plots highlight the fact that multiyear ice and odden ice are difficult to separate. The group standard errors of these two ice types overlap for most of the

81

RANGE VS ENTROPY VS LOCAL HOMOGENEITY
Smooth Data
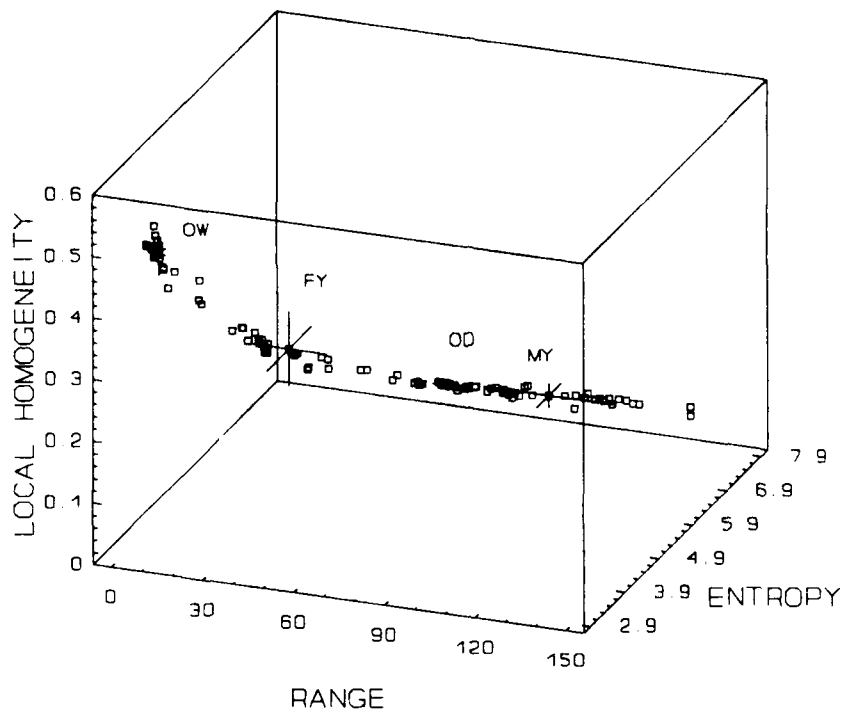
Figure 37. Top three discriminating statistics for the combination of texture and univariate statistics considering all ice types and open water samples.

statistics reviewed in this study.

The discrimination between the groups of ice and open water improves when the third variable from the stepwise discrimination is added. Plots of the top three discriminating variables for each group of statistics are seen in Figures 41-43. Note that the ice groups display the best separation when texture statistics are combined with univariate statistics (Figure 43). As may be seen from Table V, the top three univariate statistics classify the ice types and open water with greater accuracy than the texture statistics. This strong performance of the univariate statistics supports similar findings by Shuchman et al., [1989].

Table V. Discriminant Analysis Results for Original Data Set.

	TEXTURE STATISTICS	UNIVARIATE STATISTICS	TEXTURE AND UNIVARIATE STATISTICS	MULTIYEAR VERSUS ODDEN*
TOP THREE VARIABLES	Inertia (50.88%)	Range (74.56%)	Range (74.56%)	Range (81.03%)
(CUMULATIVE ACCURACY)	Entropy[b] (71.05%)	Coefficient of Variance[c] (79.82%)	Entropy (85.96%)	
	Cluster Prominence (71.05%)	Skewness[d] (79.82%)	Local Homogeneity (89.72%)	
GROUP ACCURACY	75.44%	86.84%	89.47%	94.83%

* Discriminant analysis of odden and multiyear ice was performed using both texture and univariate statistics.

[b] Unsupervised analysis would have selected Correlation as the #2 discriminator. Inertia and Correlation would have classified with 60.33% mean accuracy.

[c] Unsupervised analysis would have selected Standard Deviation as the #2 discriminator. Range and Standard Deviation would have classified with 60.33% mean accuracy.

[d] Unsupervised analysis would have selected Variance as the #3 discriminator. Range, Standard Deviation and Variance would have classified with 80.70% mean accuracy.

Within group classification accuracies were studied for each group of statistics. These tables show into which groups misclassified data fall. The within group classification accuracies appear in Table VI - VIII.

83

Figure 38. Plot of top two texture statistics, inertia and entropy, from the original data set indicates good discrimination using only two statistics for OW and FY but not for MY and OD.

RANGE VS COEFFICIENT OF VARIANCE
Original Data Set

1=FY, 2=MY, 3=OD, 4=OW
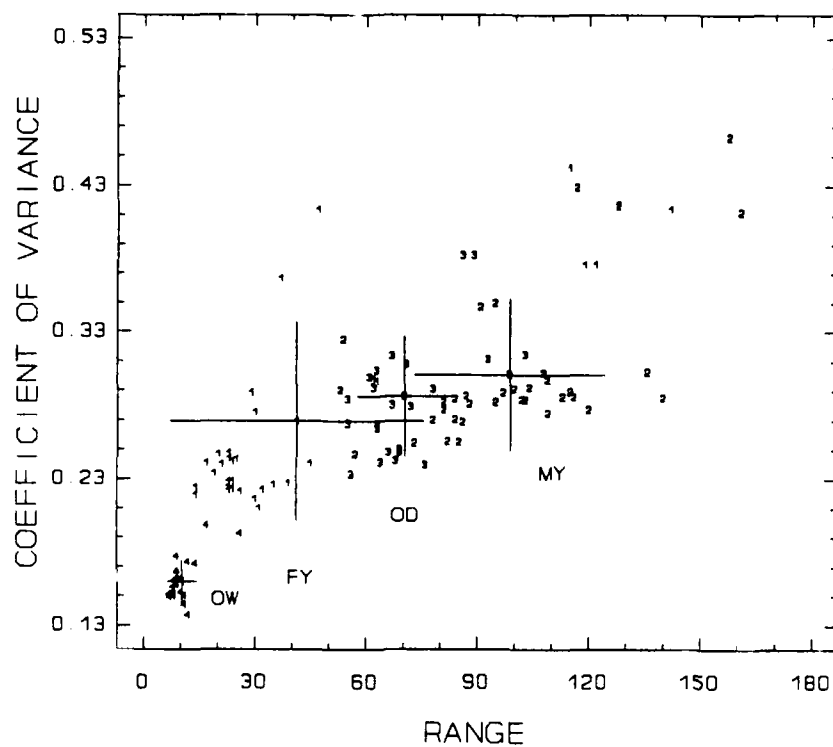
Figure 39. Plot of top two univariate statistics, range and coefficient of variance, from the original data set indicates good discrimination using only two statistics for OW and FY but not for MY and OD.

85

RANGE VS ENTROPY
Original Data Set

1=FY, 2=MY, 3=OD, 4=OW
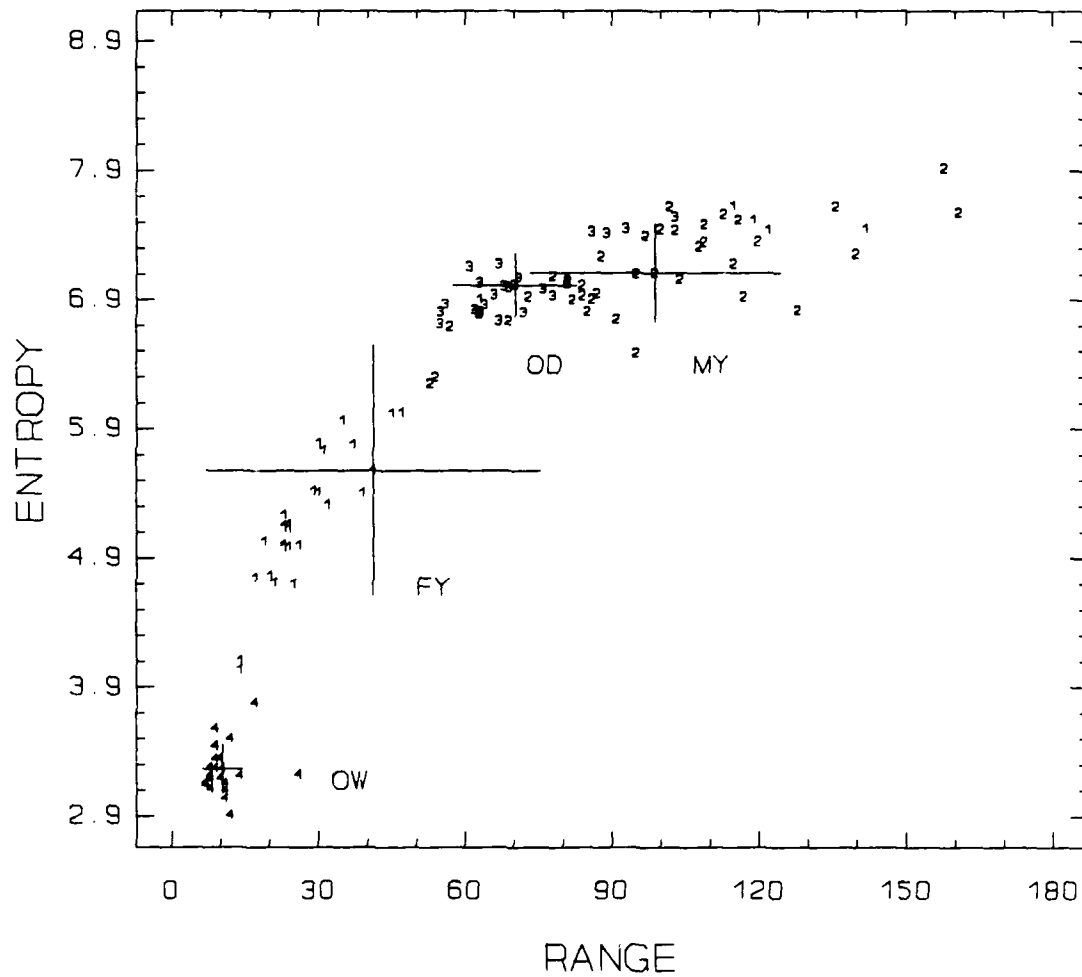
Figure 40. Plot of the top two discriminating variables, range and entropy, from the original data set indicates good discrimination using only two statistics for OW and FY. Note that the separation of OD and MY is improved.
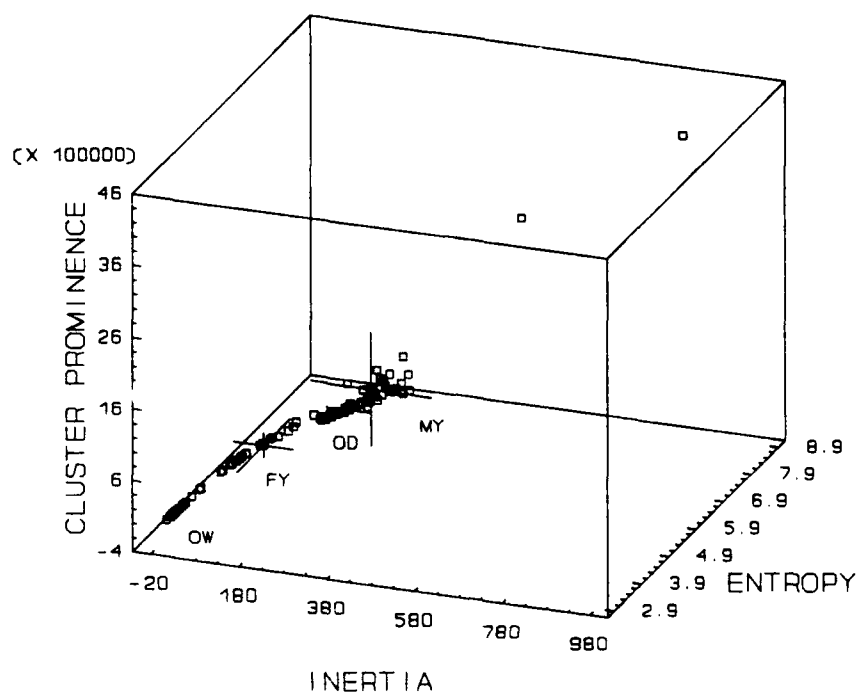
Figure 41. Plot of the top three texture statistics, inertia, entropy and cluster prominence, from the original data set indicates improved discrimination of all ice types.

87
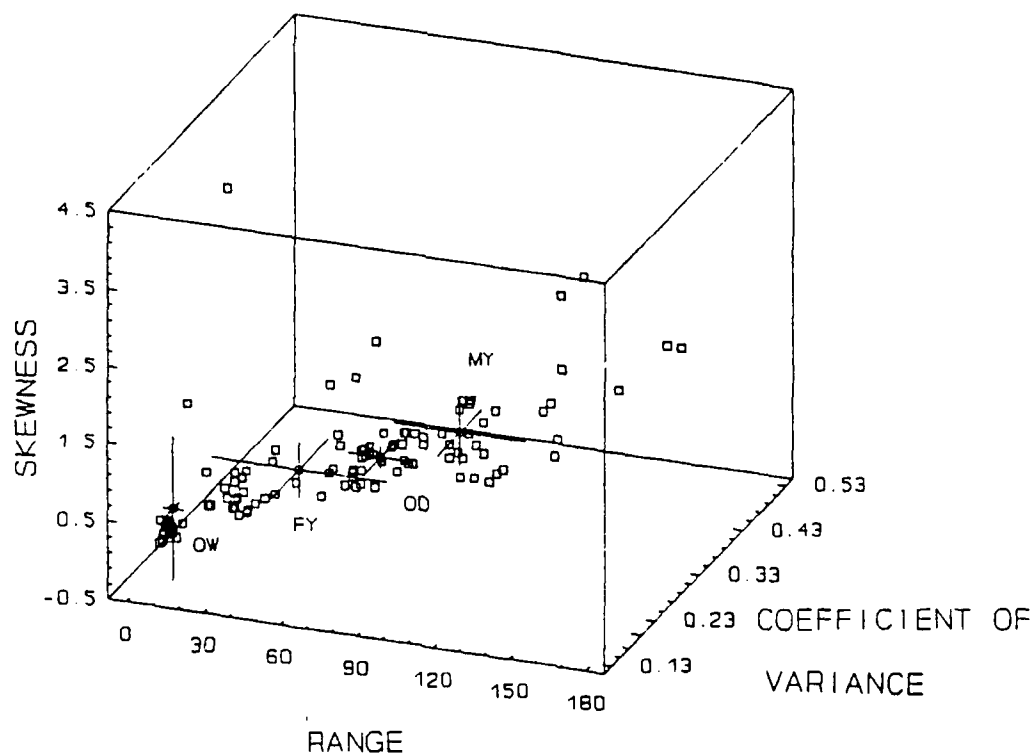
Figure 42. Plot of top three univariate statistics, range, coefficient of variance and skewness, indicate excellent separation of the groups of ice and open water for the original data set.
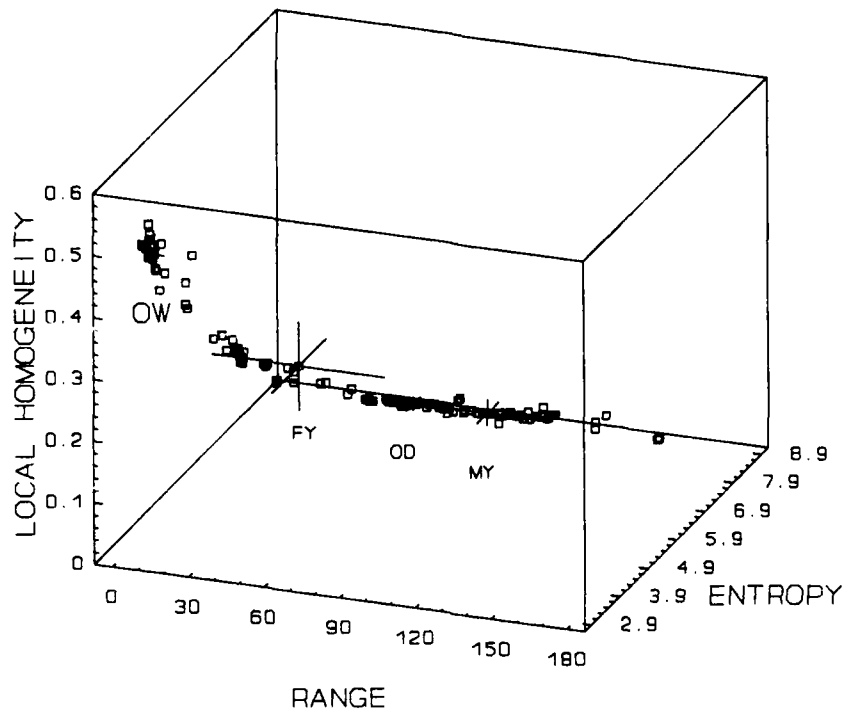
Figure 43. Plot of top three texture and univariate statistics, range entropy and local homogeneity, indicate the best seperation of any three statistics used on the original data set.

89

Table VI. Discriminant Analysis Classification Results. Texture Statistics on Original Data.

	PREDICTED GROUP MEMBERSHIP				
ACTUAL GROUP	FY	MY	OD	OW	NUMBER OF CASES
FY	26 81.3%	6 18.8%	0 0.0%	0 0.0%	32
MY	3 8.3%	29 80.6%	4 11.1%	0 0.0%	36
OD	0 0.0%	15 68.2%	7 31.8%	0 0.0%	22
OW	0 0.0%	0 0.0%	0 0.0%	24 100.0%	24
Percent of grouped cases correctly classified: 75.4%					

Table VII. Discriminant Analysis Classification Results Using Univariate Statistics.

ACTUAL GROUP	PREDICTED GROUP MEMBERSHIP				
	FY	MY	OD	OW	NUMBER OF CASES
FY	26 81.3%	2 6.3%	4 12.5%	0 0.0%	32
MY	3 8.3%	31 86.1%	2 5.6%	0 0.0%	36
OD	0 0.0%	4 18.2%	18 81.8%	0 0.0%	22
OW	0 0.0%	0 0.0%	0 0.0%	24 100.0%	24
Percent of grouped cases correctly classified: 86.8%					

Table VIII. Discriminant Analysis Classification Results. Both Texture and Univariate Statistics.

	PREDICTED GROUP MEMBERSHIP				
ACTUAL GROUP	FY	MY	OD	OW	NUMBER OF CASES
FY	26	3	3	0	32
	81.3%	9.4%	9.4%	0.0%	
MY	4	31	1	0	36
	11.1%	86.1%	2.8%	0.0%	
OD	0	1	21	0	22
	0.0%	4.5%	95.5%	0.0%	
OW	0	0	0	24	24
	0.0%	0.0%	0.0%	100.0%	
Percent of grouped cases correctly classified: 89.5%					

Open water is the most easily classified group showing perfect classification for all discriminating groups of statistics.

All groups of statistics have a tendency to misclassify odden and multiyear ice. The texture statistics (Table VI) exhibit the poorest ability to discriminate between odden and multiyear ice (31.8% accuracy). The univariate statistics perform better than texture, discriminating multiyear ice from odden ice in 81.8% of the cases. The best discrimination between odden and multiyear ice is provided by the combination of texture and univariate statistics (Table VIII). This combination classified the odden and multiyear groups with 89.7% accuracy.

V. CONCLUSIONS AND RECOMMENDATIONS

A.   CONCLUSIONS

This study has used SAR data collected during MIZEX 87 to discern the relative

strengths of texture and univariate statistics in successfully classifying SAR images of the

following ice types, first-year, multiyear, odden and open water. The following major

conclusions can be drawn:

- The choice of vector length, direction, and number used to generate a GLC matrix will effect the texture statistics. Vectors should be chosen such that the variance associated with the direction and the length is minimized. This data set revealed that three vectors of 4 pixels in length, separated by approximately 66°, removed this variance.

- The univariate statistic, range, was the single best descriptor variable. This statistic represents the minimum and maximum gray shades in an image. Range alone was capable of classifying the various ice types and open water with 74% accuracy.

- The combination of all the texture and univariate statistics provided the best classification accuracy (89.5%). When the texture statistics, entropy and local homogeneity, were combined with the univariate statistic, range, the three ice types and open water were classified with 87.7% accuracy.

- Univariate statistics as a group were better classifiers of the ice types and open water than the group of texture statistics. Range, coefficient of variance and skewness were the best three univariate statistics. These three variables were capable of classifying the ice types and open water with 79.8% accuracy.

- Multiyear ice and odden ice were the most difficult ice types to discriminate. When discrimination was performed on these two ice types, only range was a significant descriptor variable at the $p=0.01$ level of a F-ratio test for inclusion in a stepwise discrimination.

- Non-calibration of the SAR has added variance to the univariate statistics, possibly weakening the strength of the discrimination with these statistics.

B. RECOMMENDATIONS

Recommendations for future work include:

- Conduct the same analysis on another data set collected with a calibrated SAR to discern if the univariate statistic range is the strongest univariate statistic.

- Conduct a feasibility study of the added computational cost of including texture information in an algorithm. Answer the question: Is the increase in computational cost worth the gain in discrimination skill?

- Conduct the same analysis on another data set from another season of the year to compare temporal variability of the results. These results may be significantly different when melt ponds are present on the ice surface. The melt ponds may cause a significant number of images to be misclassified as open water.

- Perform an analysis on each of the textural statistics to gain a better understanding of the physical features they capture.

- Study the effect that sub-image size has on the stability of texture statistics. Establish the relationship between SAR resolution and this sub-image window size.

- Investigate how variation in polarization or SAR wavelength may be effectively used in discriminating between different ice types.

LIST OF REFERENCES

Afifi, A. A., V. Clark, Computer-Aided Multivariate Analysis, 458 pp., Lifetime Learning Publications, Belmont, 1984.

Anderson, V. H., High altitude, Side-looking Radar Images of Sea Ice in the Arctic, Proc. 4th Symp. on Remote Sensing of the Environment, Inst. of Science and Technology, University of Michigan, Ann Arbor, 845-857, April 1966.

Bezdek, J. C., (Ed.), Analysis of Fuzzy Information, Volume 1, Mathematics and Logic, 272 pp., CRC Press Inc., Boca Raton, 1987.

Bogorodskii, V. V., The Physics of Ice, 157 pp., Admin. of Hydro. Service of the Council of Ministers of the USSR., 1971.

Campbeil, W. J., R. O. Ramseier, W. F. Weeks and P. Gloersen, An Integrated Approach to the Remote Sensing of Floating Sea Ice, IAF Proceedings, Lisbon 1975.

Connors, R. W., C. A. Harlow, A Theoretical Comparison of Texture Algorithms, IEEE Trans. of Pattern Analysis and Machine Intelligence, 3, 204-222, 1980.

Doronin, Y. P., D. E. Keisin, Morskoi Led (sea ice), 323 pp., Amerind Publishing Co., New Dehli, 1977.

Glossary of Meteorology, 638 pp., American Meteorological Society, 1986.

Haralick R. M., K. Shanmugam and I. Dinstein, Textural Features for Image Classification, IEEE Trans. on Systems, Man and Cybernetics, 3, 610-621, 1973.

He, D. C., L. Wang, Texture Unit, Texture Spectrum and Texture Analysis, Proc. of IGARSS '89 Symp., Vancouver, 2769-2772, 1989.

Hoekstra, P. and D. Spanogle, Radar Cross-Section Measurements of Snow and Ice, Technial Report 235, U.S. Army Corps of Engineers, Cold Regions Research and Engineering Laboratory, Hanover, 1972.

Holmes R. A., D. R. Nuesch and R. A. Shuchman, Textural Analysis an Real-Time Classification of Sea-Ice Types Using Digital SAR Data IEEE Trans. on Geoscience and Remote Sensing, 22, 113-120, 1984.

Holyer, R. E., A Global Approach to Image Texture Analysis, Ph.D. dissertation, 264 pp., Univ. of South Carolina, Columbia, 1989.

Johnson J. D., and L. D. Farmer, Use of Side-Looking Air Borne Radar for Sea Ice Identification, J. Geophys. Res., 76, 2138-2155, 1971.

Kachigan, S. K., Multivariate Statistical Analysis, 297 pp., Radius Press, New York, 1982.

Ketchum R. D., Dual Frequency Radar Ice and Snow Signatures, Naval Ocean Research and Development Activity, Bay St. Louis, AD-A115297, December 1981.

Lewis, E. O., B. W. Currie, S. Haykin, Detection and Classification of Ice, 325 pp., Research Studies Press, Letchworth, Hertfordshire, England, 1987.

Moore, R.K., Radar Scatterometry-An Active Remote Sensing Tool, Rep. NASA-CR-77756; CRES-61-11, 41 pp., Kansas Univ., Lawrence, 1966.

Pounder, E. R., Physics of Ice, 151 pp., Pergamon Press Ltd. London, 1965.

Rosenfield, A., Visual Texture Analysis: An overview, University of Maryland, Computer Science Technical Report Series, TR-406, College Park, August 1975.

Rouse J. W., Arctic Ice Type Identification By Radar, Proc. of the IEEE., 57, 605-611, 1969.

SAR (Synthetic Aperture Radar), Earth Observing System, Volume IIf, Instrument Panel Report, NASA-TM-89701, 260 pp., National Aeronautics and Space Administration, Greenbelt, MD., Goddard Space Flight Center, 1987.

Shanmugam S., V. Narayanan, V. S. Frost, J. A. Stiles and J. C. Holtzman, Textural Features for Radar Image Analysis, IEEE Trans. on Geoscience and Remote Sensing, 19, 155-156, 1981.

Shokr, M. E., Texture Measures for Sea-Ice Classification from Radar Images, Proc. of IGARSS '89 Symp., Vancouver, 763-768, 1989.

Shuchman, R. A., L. L. Sutherland, B. A. Burns, E. D. Leavitt, MIZEX 1987 SAR, Data Summary, ERIM report 154600-34-T, 126 pp., Informal Information Report to Office of Naval Research, Arctic Science Program, Arlington, February 1988.

Shuchman, R. A., C. C. Wackerman, A. L. Maffett, R. G. Onstott, and L. L. Sutherland, The Discrimination of Sea Ice Types Using SAR Backscatter Statistics, Proc. of IGARSS '89 Symp., Vancouver, 381-385, 1989.

Stewart, R. H., Methods of Satellite Oceanography, 360 pp., University of California Press, Berkeley, 1985.

Sutherland, L. L. and R. A. Shuchman, SAR and Passive Microwave Observations of the Odden During MIZEX '87, Proc. of IGARSS '89 Symp., Vancouver, 1539-1543, 1989.

Tabachnick, B. G., L. S. Sidell, Using Multivariate Statistics (2ed.), 746 pp., Harper and Row, New York, 1989.

Timokhov, L. A., Dynamics of Ice Cover, 219 pp., Gidrometeoizdat Publishers, Leningrad, 1974.

Trivedi, M. M., C. A. Harlow, R. W. Conners and S. Goh, Object Detection Based On Gray Level Co-Occurrence, Computer Vision. Graphics. and Image Processing, 28, pp. 199-219, 1984.

Untersteiner, N., (Ed.), The Geophysics of Sea Ice, 1196 pp., Plenum Press, New York, 1986.

Vant, M. R., R. B. Gray, R. O. Ramseier, and V. Makios., Dielectric properties of fresh and sea ice at 10 and 35 GHz., Journal of Applied Physics, 45, 4712-4717, 1974.

Websters Ninth New Collegiate Dictionary, 1563 pp., Mirriam Webster Inc. Publishers, Springfield Mass., 1983.

Wadhams, P., The Ice Cover, in The Nordic Seas, ed. by Hurdle, B. G., p. 21-84, Springer-Verlag, New York, 1986.

Weeks, W. F. and S. F. Ackley, The Growth, Structure, and Properties of Sea Ice, CREEL Monograph 82-1, 130 pp., November 1982.

Weszka, J. S., C. R. Dyer and A. Rosenfield., A Comparative Study of Texture Measures for Terrain Classification, IEEE Trans. on Systems, Man and Cybernetics, 6, 269-285, 1976.

WMO, Sea-Ice Nomenclature, WMO/OMM/BMO-No.259.TP.145, 147 pp., 1970.

INITIAL DISTRIBUTION LIST

No. Copies

1. Defense Technical Information Center   2
   Cameron Station
   Alexandria, VA 22304-6145

2. Library, Code 0142   2
   Naval Postgraduate School
   Monterey, CA 93943-5000

3. Chairman (Code OC/Co)   1
   Department of Oceanography
   Naval Postgraduate School
   Monterey, CA 93943-5000

4. Chairman (Code MR/Rd)   1
   Department of Meteorology
   Naval Postgraduate School
   Monterey, CA 93943-5000

5. Superintendent
   Naval Postgraduate School
   Attn: Dr. R. H. Bourke, Code OC/Bf   1
          Dr. J. A. Nystuen, Code OC/Ny   2
   Monterey, CA 93943-5000

6. LCDR F. W. Garcia Jr.   1
   Commander Amphibious Group Two
   Fleet Post Office
   NY 09501-6007

7. Director Naval Oceanography Division   1
   Naval Observatory
   34th and Massachusetts Avenue NW
   Washington, DC 20390

8. Commander   1
   Naval Oceanography Command
   Stennis Space Center,
   MS 39529-5000

99

9. Commanding Officer   1
Naval Oceanographic Office
Stennis Space Center,
MS 39522-5001

10. Commanding Officer   1
Fleet Numerical Oceanography Center
Monterey, CA 93943-5005

11. Commanding Officer   1
Naval Oceanographic and Atmospheric
Research Laboratory,
Stennis Space Center,
MS 39529-5004

12. Commanding Officer   1
Naval Oceanographic and Atmospheric
Research Laboratory, Code 321
Ocean Sensing and Prediction Division,
Remote Sensing Branch,
Stennis Space Center,
MS 39529-5004

13. Commanding Officer   1
Naval Oceanographic and Atmospheric
Research Laboratory,
Monterey, CA 93943-5006

14. Chairman, Oceanography Department   1
Attn: Dr. R. J. Holyer
U. S. Naval Academy
Annapolis, MD 21402

15. Chief of Naval Research   1
800 N. Quincy Street
Arlington, VA 22217

16. Office of Naval Research (Code 420)   2
Attn: Dr. C. K. Luther
800 N. Quincy Street
Arlington, VA 22217

17. Library   1
P. O. Box 2367

Scripps Institution of Oceanography
La Jolla, CA 92037

18. Library   1
    Department of Oceanography
    University of Washington
    Seattle, WA 98105

19. Library   1
    CICESE
    P. O. Box 4803
    San Ysidro, CA 92073

20. Library   1
    School of Oceanography
    Oregon State University
    Corvallis, OR 97331

21. Commander   1
    Oceanographic Systems Pacific
    Box 1390
    Pearl Harbor, HI 96860

22. Commander (AIR-370)   1
    Naval Air Systems Command
    Washington, DC 20360

23. Chief, Ocean Services Division   1
    National Oceanic and Atmospheric
    Administration
    8060 Thirteenth Street
    Silver Springs, MD 20910

24. Environmental Research Institute of Michigan   1
    Attn: Dr. C. C. Wackerman
            Dr. L. L. Sutherland
    P. O. Box 8618
    Ann Arbor, MI 48107-8618

25. U.S. Army Corps of Engineers, CRREL   2
    Attn: Library
            Dr. D. Farmer
    Hanover, NH 03755-1290

27. Commanding Officer   1
     Naval Polar Oceanography Center, Suitland
     Washington, DC 20373

28. Jet Propulsion Laboratory   1
     California Institute of Technology
     Attn: Dr. B. Holt
     4800 Oak Grove Drive
     Pasadena CA 91109

29. Superintendent   1
     Code 012
     Naval Postgraduate School
     Monterey, CA 93943-5000